V BB

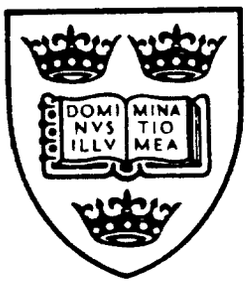

UNIVERSITY OF OXFORD

Department of Physics

PARTICLE AND NUCLEAR PHYSICS

INVESTIGATIONS INTO THE ORIGIN OF THE SPURIOUS 17 keV NEUTRINO SIGNAL OBSERVED IN ^{35}S BETA DECAY

M.G. Bowler and N.A. Jelley

Ref: OUNP-95-02

Address: Department of Physics
Particle & Nuclear Physics
Keble Road
Oxford OX1 3RH
U.K.

Investigations into the origin of the spurious 17 keV neutrino signal observed in ^{35}S beta decay

M.G. Bowler and N.A. Jelley

Nuclear Physics Laboratory, University of Oxford
Oxford OX1 3RH

Abstract

An exhaustive study has been made of the β spectrum of ^{35}S, recorded with a Si(Li) detector. The object was to identify the origin of the significant distortion in the ^{35}S β spectrum some 17 keV below the end point, reported over three years ago and interpreted then as evidence for a 17 keV neutrino. Measurements with different source-detector spacings and with varied collimation have shown that the long range curvature of the Kurie plot is a sensitive function of configuration and that the long range component of the electron response function cannot be predetermined with sufficient accuracy. The principal origin of the distortion is however energy loss in the ^{35}S sources. The ^{35}S sources, prepared by chemical adsorption of $Ba^{35}SO_4$ on a gold substrate, are clumped and locally thick. Electrons near the end point lose $\sim$ 0.3 keV in the source material and if this is taken into account the spectra are well fitted without any admixture of 17 keV neutrino. The source thickness has been investigated with a proton microprobe and determined from both source tilting and the yield of barium K X-rays; these studies are discussed in detail. The uncertainties in and justification for the form of the electron response function employed are also thoroughly discussed.

If there is no systematic error common to the majority of 14 independent sets of ^{35}S data, the admixture of 17 keV neutrino is $< 10^{-3}$ (95% CL). A simple search for a kink at 150 keV in the combined data from all 14 runs yielded a limit of 1.8×10^{-3} (95% CL). The end point of the ^{35}S β spectrum is found to be 167.60 ± 0.05 keV.

1. Introduction.

1.1 A brief history.

In 1985 Simpson reported an excess of counts below 2 keV in the β spectrum of tritium implanted in a Si(Li) solid state detector [1]. This excess was consistent with a superposition of two electron spectra, a dominant component characteristic of a massless neutrino ν_l and a second corresponding to emission of electrons accompanied by a neutrino of mass $\sim 17\,\mathrm{keV}$, ν_h. These data were interpreted as evidence that the electron neutrino is a mixture of two components

$$\nu_e = \nu_l \cos\theta + \nu_h \sin\theta$$

with $\sin^2\theta \sim 0.03$. There followed a flurry of experiments on a different β emitter, ^{35}S, using both magnetic spectrometers [2–4] and solid state detectors [5,6]. All these experiments yielded null results and in some cases very stringent limits were claimed. It was also pointed out (see [11]) that corrections to the screening potential and exchange effects in atomic tritium would reduce the excess of low energy counts reported in [1] and approximately halve the inferred 17 keV neutrino admixture. The negative ^{35}S experiments were cogently criticised by Simpson [7], Simpson and Hime [8] and later by Bonvicini [9]. With the benefit of hindsight one can reasonably conclude that while those experiments might have detected a 3% admixture it is doubtful that they excluded a 1% admixture of 17 keV neutrino. A very careful report of an experiment on ^{63}Ni appeared in 1987, again negative and claiming an upper limit of 0.3% (90%CL) [10].

The tritium spectrum was re-examined by Hime and Simpson, the tritium being implanted in a hyperpure germanium detector. Excess counts were again observed at low energy and best described by an admixture of a 17 keV neutrino with $\sin^2\theta$ between 0.6% and 1.6%, when allowance was made for uncertainty in the effective screening potential [11]. Simpson and Hime also carried out an experiment on ^{35}S using a Si(Li) detector placed in front of a source prepared by precipitation of $Ba^{35}SO_4$ from a drop of $Na_2{}^{35}SO_4$ solution. The β spectrum showed a distortion near the end point fitted with 0.73% of 17 keV neutrino [8].

In an attempt to improve on [8] Hime and Jelley undertook a ^{35}S experiment which also employed an external source prepared by chemical deposition of $Ba^{35}SO_4$. The source was placed further away from the Si(Li) detector than in [8] and collimated so that electrons were incident on the detector within 10° of the normal and did not reach the edge of the detector. The electron response function was constructed from Monte Carlo calculations and from measurements of internal conversion (IC) lines from sources of ^{57}Co and ^{109}Cd, precipitated as hydroxides. The ^{35}S β spectrum was distorted near the end point and that distortion fitted with 0.8% of 17 keV neutrino. A significance of ~ 8 standard deviations was claimed for each of two runs [12]. At about the same time a positive result was reported from a completely independent experiment, ^{14}C dissolved in a germanium detector [13]. These new positive results generated intense, though shortlived, interest in 17 keV neutrino physics [14]. It rapidly became clear that, far from providing an explanation of missing mass in the

universe and the solar neutrino problem, a 17 keV neutrino is completely inconsistent with cosmological data unless it decays both rapidly and invisibly. Such schemes as have been devised require major and rather ad hoc extensions to the standard model [15]. It was essential to settle the question of the existence of the 17 keV neutrino by more experiments on β spectra and, confident that a number of completely new and independent experiments would be undertaken, we resolved to work with the apparatus and techniques of the Oxford ^{35}S experiment [12] and search for a mundane explanation of the distortion near the end point, for the data of [12] constituted apparently by far the strongest evidence for the existence of a 17 keV neutrino. In undertaking this thankless task we were influenced by the negative result of [10].

By early 1992 opinion was hardening against the existence of a 17 keV neutrino, exemplified by the review [16] at the XIIth Moriond Workshop. That review contains the negative preliminary results of a very high statistics experiment on ^{63}Ni [18] and at the same meeting the electron response function of [12] was criticised [17]. At the Granada conference "Neutrino 92" [19] negative results from a number of high precision experiments were discussed. More negative results were reported early in 1993 at the XIII Moriond Workshop [20], at which Hime, following [17], reported that the inclusion of the effects of scattering off an intermediate baffle largely removed the significance of the results of [12]. At the same meeting we reported preliminary conclusions to the effect that [12] could not be taken as positive evidence for a 17 keV neutrino because allowance for scattering and an increased energy loss tail completely eliminated the distortions in our data. We did not know at that time whether our ^{35}S data were really affected by extra energy loss.

High precision results from the study of β spectra near the end point have now been reported from a number of experiments and the results are all negative (see table 1.1). In addition to [18] the experiment reported in [21] used ^{63}Ni and a high precision magnetic spectrometer. Measurements of the spectrum of ^{35}S with magnetic spectrometers are reported in [22] and in [23], which includes a re-analysis of the data of [2]. An experiment on ^{35}S, carried out with a solid state detector, used a magnetic field to guide electrons from source to detector and to partially suppress back scattering from the detector [24]. Another ^{35}S experiment employed a very thin source between two silicon detectors in a magnetic field; summing the signals from the two detectors gave virtually total suppression of back scattering [25]. All these recent experiments used magnetic fields to transport the electrons and so are vulnerable to the suggestion that there is an outside chance that the presence of a magnetic field suppresses production of a 17 keV neutrino [26]. Our own experiments have enabled us to identify the origin of the distortion of the β spectrum of ^{35}S, previously attributed to a 17 keV neutrino, and incidentally to set a stringent limit. Magnetic fields were not employed.

The results of the recent β experiments are summarised in table 1.1.

1.2 The present experiments.

The present experiments commenced at the end of 1991 and by the end of 1993 we had accumulated ^{35}S data from a total of 14 runs of typically 8 days

each. We used three different ^{35}S sources and varied the source-detector distance by factors of 1.5 and 2. The collimation was also varied and the rate at which data were taken ranged from 2 kHz to 8 kHz. Very early on we studied pileup by running a pulser above the end point of the ^{35}S spectrum and discovered a low energy pileup toe extending to $\sim$ 11 keV above the pulser peak, caused by the threshold of the active pileup rejection unit for small signals. This was not suspected in the original work [12] and under the conditions of that work would have produced $\sim$ 10% of the observed distortion. After a few runs it became clear that long range curvature of the Kurie plot is a sensitive function of the geometry of source, detector and collimators and corresponding effects were seen in the tail of the electron response function determined with ^{109}Cd IC lines. We took this as evidence that some electrons reach the detector after intermediate scattering or penetration of the edges of collimators. Removal of this long range curvature, either by addition of a constant component to the electron response function or with a low order polynomial shape factor, invariably left a characteristic kickup in the residuals near the end point, which passed upwards through zero just below 160 keV and exceeded 10% of the signal as the end point was approached. It is such a distortion which constituted the primary evidence for a 17 keV neutrino in [12]. We found, purely empirically, that if the energy loss experienced by ^{35}S electrons were greater by a factor of 1.5–2 than that determined from ^{109}Cd lines then the residuals flattened out and no distortion remained. By late 1992 we were able to report [20] the weak conclusion that the data of [12] could no longer be regarded as constituting positive evidence for a 17 keV neutrino.

The additional energy loss required amounts to $\sim$ 0.3 keV at the end point. It is not obvious that this can violently distort the residuals over the last 10 keV of the β spectrum, but the effect is easily understood (section 5.1). We found that this distortion, of short range in energy, could not be produced by relatively long range effects such as scattering, aperture penetration or back diffusion of electrons from the source and eliminated the possibility that extra energy loss was the result of ice building up on the ^{35}S source during the runs. There remained the possibility that the Ba^{35}SO$_4$ sources are clumped and locally thick. This was indeed indicated by studies of proton induced barium L X-ray emission, carried out with the Oxford proton microprobe on a piece of a dying source, and confirmed with the β spectrometer by the time honoured technique of tilting a source which was very much alive. Finally we extracted a barium K X-ray signal from the accumulated runs and found the effective thickness of barium in the source seen by ^{35}S electrons. All these measurements were entirely consistent with the mean source thickness necessary to remove the distortion near the end point of ^{35}S and all 14 runs rejected the hypothesis of a 17 keV neutrino admixture in favour of that of a thick source. The apparent evidence for a 17 keV neutrino in the ^{35}S β spectrum arose primarily because in [12] the sources were assumed to be thin. If there is no systematic effect common to the majority of our runs, we find $\sin^2\theta < 0.1\%$ (95%CL).

A brief account of this work has already been published [27]. The purpose of the present paper is to give a thorough account of our work, in far more detail than was possible within the confines of [27]. We display our data and

relevant conditions run by run and also discuss in detail the extraction of the thickness of the sources from our tilting and X-ray studies (in neither case is it entirely straightforward), the studies of pileup and the effects of scattering on the electron response function. Since our work has finally demolished what was at one time by far the most convincing evidence for the existence of a 17 keV neutrino [12], we think it proper that these details are available for scrutiny. We have also taken the opportunity to correct a few unimportant errors in [27] and to present the results of some work done since the publication of [27]; in particular a simple search of the combined data from all 14 runs for a kink at $\sim$ 150 keV. This yielded a limit on the admixture $< 0.18\%$ (95% CL) and is both independent of assumptions concerning the electron response function and insensitive to possible systematic errors, because any such effects would be smooth.

2. Apparatus

2.1 Spectrometer

We deliberately employed the same apparatus as in [12], described in more detail in [29], an ORTEC liquid nitrogen cooled thin window Si(Li) detector 5 mm thick and with an active area of 200 mm^2, supplied with a cooled FET package and feedback circuit to optimise resolution. Radioactive sources were deposited on thin foils and mounted in vacuum parallel to the face of the detector. The principal features of the apparatus are illustrated in fig.2.1. A 2 mm thick aluminium collimator with an aperture of diameter 10 mm was mounted 10 mm in front of the gold contact of the detector, chamfered at an angle of 10°. This collimation of the detector was used in all the runs but one, 13. In this run a composite baffle provided a 2 mm thick copper detector collimator with an aperture of diameter 6 mm chamfered at an angle of 30°. Other collimators and baffles were mounted on the source carriage, which consisted of four long aluminium rods screwed at one end to a base plate and at the other to an aluminium ring. To this was screwed a chamfered teflon ring and between the two rings antiscatter baffles were mounted, in most cases 0.8 mm aluminium rings. The base plate was mounted on a linear motion feed through — the whole source carriage was withdrawn from the detector vacuum chamber, which was then isolated with a gate valve, when sources were changed without warming the detector. The teflon ring on the end of the source carriage engaged a tapered sleeve which directed the snout to centre when the carriage was wound forward again. The four aluminium rods carried the source holder and (usually) a copper source collimator 1 mm thick, mounted 3 mm in front of the source foil. The aperture of this collimator was varied between 3 mm and 8 mm in this series of experiments and data were taken with sources at distances of 56, 84 and 112 mm from the detector contact. The aluminium rods of the source carriage were also used to support holders enabling the sources to be tilted.

In the majority of our runs the 0.8 mm aluminium antiscatter baffle had an aperture of 31 mm diameter and was chamfered, facing the source, to a knife edge at an angle of 67° to the axis. In three runs the aperture was 26 mm in

diameter and flat, perpendicular to the baffle faces, as in [12]. Details of the geometry and collimation employed in each of our runs are given in section 4.1.

The vacuum chamber was maintained at $\sim 8 \times 10^{-8}$ mbar, using an oil diffusion pump with a liquid nitrogen cold trap. A cylindrical panel cooled with liquid nitrogen completely surrounded the inner part of the detector chamber and was in thermal contact with the detector collimator. This large cold surface was intended to freeze out any residual water vapour and prevent the buildup of ice on the detector. However, we never succeeded in completely eliminating the buildup of ice on the detector, the effects of which were manifested in several ways. Before and after each ^{35}S run, ^{109}Cd spectra were taken. An increase of ice on the detector lowered the peak positions of K, L, M IC lines and L Auger lines and increased the tail due to energy loss. The β spectrum of ^{35}S is greatest at zero energy and drops smoothly to the end point, but in the presence of energy loss the measured spectrum exhibits a broad peak at low energy. The energy of this peak invariably increased during the course of each ^{35}S run. The buildup of ice (typically $\sim 50\mu$g cm^{-2} over 8 days) did not constitute a problem, because it was measured with ^{109}Cd, and proved a blessing in disguise, for these measurements provided the calibration for determining source thickness through tilting the source foil (section 6.4).

The same ORTEC 672 main amplifier was used and, as in [12], operated with a shaping time of 3μs. Unipolar pulses were fed into the same Silena ADC in coincidence with logic pulses from the 672 active pileup rejection unit. The spectra were recorded with the same CATO MCA, but we utilised 4096 channels at a dispersion of 77 eV/channel.

In the interval between the end of the experiments carried out by Hime and Jelley and the beginning of our work, the detector used in [12] had been returned to the manufacturers for servicing, following an accident with a beryllium window. It was not resurfaced and we used this detector in the first two runs of our work, but with a new 139-2 preamplifier. Before experiments commenced, we had observed deterioration of the contact layer on the original detector and although the performance had not apparently deteriorated, we replaced it with a new one after the first two runs and used the new detector throughout the rest of our work.

2.2 Calibration

The linearity of the electronics was established with a precision pulser (BNC PB-4) and the system calibrated, run by run, with γ and X-rays from ^{109}Cd and checks made with ^{57}Co sources. The response of the system to the full energy of γ and X-rays was well represented by a gaussian form with an energy dependent variance of form $a + bE_\gamma$, such that the full width at half maximum was 650 eV at 100 keV and 790 eV at 170 keV, the latter corresponding to ~ 10 ADC channels. We found only three potentially troublesome features of the electronics. First, an ADC stagger every four channels at a level of $\sim 0.1\%$; this was trivially removed by summing in groups of 4 or 8 channels. Secondly, the recorded MCA ^{35}S spectra exhibited a violent but rapidly damped oscillation from the low energy cutoff (~channel 60) to ~channel 120 (9 keV). This was of no significance for our analyses of the ^{35}S spectrum over the range 100–200 keV,

but when necessary was removed in studies of the low energy end of the ^{35}S spectra by dividing by the recorded spectra of a ramped pulser, which exhibited the same oscillations. Finally, we discovered substantial pileup of the low energy part of the ^{35}S spectrum ($\lesssim 11$ keV), measured by operating a pulser well above the ^{35}S endpoint.

2.3 Pileup

The Ortec 672 amplifier, used in this work and in the original experiment, incorporates a pileup rejection unit. After a pulse has been detected in the output from a fast amplifier, that output is inspected for a second pulse. If such a pulse is detected within the inspection interval a reject signal is generated. When the reject signal precedes peak detection in the Silena ADC both pulses are rejected, but if peak detection occurs before the reject signal then only the second pulse is rejected. This system fails if two pulses arrive within the pulse duration of the fast amplifier (~ 350 ns), in which case the signal processed by the ADC is the linear sum of the two pulses. This sum pileup did not occur at a rate exceeding 0.5% in these experiments and the rate was determined, run by run, from the ^{35}S data themselves.

However, the pileup rejection fails in another way which is potentially more dangerous. A pulse is only detected if it exceeds a threshold which is automatically set just above the noise level in the fast amplifier and the minimum detectable signal is limited by the detector and preamplifier noise characteristics. Thus a second pulse will be added to the first, regardless of when it occurs within the inspection interval, if the second is sufficiently small. We studied this effect with two asynchronous pulsers, the first of which produced a relatively large signal. Adding a signal from the second pulser which corresponded to greater than 11 keV in the detector resulted only in a sum pileup peak, but as the second signal was reduced the space between the higher signal and the sum peak filled in progressively. The first 11 keV of the β spectrum thus piles up at a much greater rate than for sum pileup alone and such an effect distorts the β spectrum near the end point.

The pileup of the first 11 keV was studied with the simple expedient of taking ^{35}S data with a pulser simultaneously producing a peak well above the end point of the β spectrum. The effect is illustrated in fig.2.2 for a pulser run following run 3; it shows a little of the high energy side of the pulser peak and the pileup of the ^{35}S β spectrum on the pulser signal. The low energy pileup generates an approximately triangular toe which reaches 145 channels (11 keV) above the centre of the pulser peak, after which there remains only sum pileup. We represented the toe pileup by a form suggested by the results of the studies with two pulsers

$$n(N) = \frac{n_0}{N_c} \ln \frac{N_c}{N} \tag{2.4.1}$$

where N_c is the number of channels above the pulser peak at which toe pileup merges into sum pileup, $n(N)$ is the contents of channel N above the pulser peak and n_0 represents the number of toe pileup counts. The toe pileup fraction is defined to be n_0/N_p, where N_p is the number of counts in the pulser peak.

For the data shown in fig.2.2, N_p was 3×10^6 and n_0 1.86×10^4, yielding a low energy pileup fraction of 0.62% at a rate of 5.9 kHz. The toe pileup fraction varies linearly with the β rate, as expected, and this variation is shown in fig.2.3.

The effect of the toe pileup on the β spectrum is to introduce a distortion near the end point of form very similar to that reported in [12] and there interpreted as evidence for a 17 keV neutrino. However, toe pileup would have to be present at a level of several per cent to be responsible for the whole. In most of our runs and for the conditions of the original experiment, the fraction of low energy pileup is a factor ~ 10 lower than necessary to account for the distortion.

In the calculation of pileup the measured toe was used for pileup of the β spectrum below 11 keV and the sum pileup calculated only for electrons above 11 keV. Once determined, neither form of pileup constitutes a problem, but in the original experiment pileup of signals below 25 keV was not studied and the existence of the toe remained unsuspected [29,30].

2.4 Source preparation.

The sources used in [8] and in [12] were prepared by a technique of chemical adsorption, following [28]. That paper, entitled Ultra-thin Radioactive Sources, describes how sources were made by adsorption of the insoluble hydroxides of the alpha emitters ^{241}Am and ^{244}Cm and makes the point that the more common inactive impurities in solutions do not form insoluble hydroxides. Sources of thickness $< 1\mu$g cm^{-2} were evidently prepared. The preparation of the sources used in [12] is described in detail in [29]; we followed the same procedure.

Mylar foils $\sim 3\mu$m thick, bearing an evaporated layer of gold 100 Å thick, were used as the source substrates. These foils were clamped between two aluminium rings of internal diameter 2 cm. A recessed O ring in the lower disc stretched the mylar taut and the gold layer was in electrical contact with the upper aluminium ring. A drop of $Na_2{}^{35}SO_4$ solution (prepared by Amersham International, using water of injectable quality) was deposited on the gold and a drop of $Ba(NO_3)_2$ of higher concentration added. The gestating source was left on an island surrounded by $Ba(NO_3)_2$ solution, in a closed container, for ~ 1 hr. At the end of that time the liquid was drawn off and the source washed several times. For each wash, one or more drops of distilled water were deposited on the gold to cover the area of precipitate, left for ~ 1 min and then drawn off. We found these washes extremely effective in removing dried $Na_2{}^{35}SO_4$ from a gold surface. The desired end was a monomolecular layer of insoluble $Ba^{35}SO_4$ held to the gold of the substrate. Sources of ^{109}Cd and ^{57}Co were precipitated as hydroxides with KOH from solutions in weak HCl. At all stages the liquids were deposited by hand, using hypodermic syringes, and the area of contact was seldom either circular or precisely centred.

We made autoradiographs of both ^{35}S and ^{109}Cd sources, by placing discs of photographic emulsion in contact with the sources. Contact could not be perfect and we could only gain qualitative information, but in both cases it was clear that the radioactive material was very far from uniformly deposited — the autoradiographs were very spotty and some of the spots evidently hot. We eventually determined by other means that the ^{35}S sources, prepared by precipitation of sulphates with $Ba(NO_3)_2$, are clumped and locally thick (sections 6.4,

7.1), but that ^{109}Cd sources, precipitated as the hydroxide, are relatively thin, $< 30\mu$g cm^{-2} (section 6.3).

The first ^{35}S source (#1) had an initial activity $\sim 40\mu$Ci. By the end of the first two runs the count rate had dropped to ~ 2 kHz and after installing the second detector we prepared #2 from a stronger solution of $Na_2{}^{35}SO_4$. This had an initial activity $> 300\mu$Ci and it was necessary to place it far back from the detector (112 mm) or use a 3 mm diameter source collimator in order to reduce the initial count rate to ~ 8 kHZ — above this rate charge built up too fast and the front end electronics shut down.

Source #3 ($\sim 20\mu$Ci) was made by a different technique, in an unsuccessful attempt to produce a locally thin ^{35}S source. This is described in section 6.4.

3. Electron response function.

3.1 Introduction

The response of the detector to monoenergetic electrons is complicated by the effects of energy loss in the gold contact (200 Å) and in the dead layer beneath it and by back scattering from the detector; electrons scattered out of the detector do not deposit their full energy. These effects were the only ones considered in [12], but subsequent to that work it was pointed out that electrons degraded in energy may reach the detector as a result of scattering from intermediate surfaces, penetration of the edges of apertures and back diffusion from the source substrate [17,34]. In the case of ^{35}S, we have found that energy loss within the source material is also important. The model electron response function must be able to accommodate all these effects. Energy loss is well understood and there is a deal of information on the effect of saturation back scattering from silicon detectors [31–33] which supports the Monte Carlo calculations in [12]. We doubt that calculations of the effects of intermediate scattering, aperture penetration and back diffusion [17,34] can be more than indicative. We represented the electron response function with a term for energy loss (section 3.2), a term for the effect of backscattering from the detector (section 3.3), and a flat component independent of deposited energy up to the full energy (section 3.4).

The electron response function might in principle be determined with monoenergetic IC lines from sources prepared in the same way as β sources. The shape of the tail due to energy loss can certainly be determined this way but, as we discovered, the content as opposed to the shape depends on source thickness. The long range tail, due to back scattering from the detector and other effects contains a fraction approximately independent of energy and with shape an approximately constant function of the fractional energy — for a given number of IC electrons, the content of any bin in the long range tail falls linearly with increasing energy of the IC line. There is also a background due to γs from the IC source which are Compton scattered into the detector from nearby material; this must be subtracted using runs with the electrons screened out [29]. It is thus difficult to determine accurately the long range tail of the electron response function using ^{57}Co, which has γs at 122 and 136 keV with K conversion coefficients

of 0.022 and 0.136 respectively; we could not constrain the flat component significantly from ^{57}Co spectra. Background problems are much reduced with ^{109}Cd, which has a single γ at 88 keV with K and L internal conversion coefficients ~ 11. We determined the electron response function for ^{109}Cd and used ^{57}Co merely to check the energy dependence of the energy loss term; we found that the energy loss determined from ^{57}Co IC lines was a factor 1.046 ± 0.005 greater than that determined from three ^{109}Cd lines, extrapolated assuming the energy loss tail to be inversely proportional to the square of the electron speed. We achieved good representations of the ^{109}Cd data, illustrated in fig.3.1, but found we had not thereby determined the response function appropriate to electrons near the end point of ^{35}S.

3.2 Energy loss component

The differential cross section for energy loss by collision with a free electron, given by the Rutherford formula, is

$$\frac{d\sigma}{dT'} = \frac{2\pi e^4}{mv^2}\frac{1}{T'^2} \tag{3.2.1}$$

where v is the speed of the incident particle, m the electron mass and T' the energy transferred to the struck electron. For (non-relativistic) heavy particles the maximum energy transfer in a single collision is the small fraction $4m/M$ of the incident kinetic energy, but for electrons the full energy can be transferred. The probability that an electron loses energy $> T'_c$ in passing through a thin layer of material is

$$\Delta P \simeq \frac{2\pi e^4}{mv^2}\frac{1}{T'_c} N \Delta x \tag{3.2.2}$$

where N is the electron density and Δx the thickness of the layer. If ΔP is small, the energy loss spectrum will exhibit a long inverse square tail beyond T'_c. In our experiments the probability of ^{109}Cd K electrons losing more than 1 keV in a single collision was $\approx 10\%$. The energy resolution was ~ 0.7 keV (FWHM) and we modelled the effect of energy loss by a peak shift Δ and a tail. The peak shift absorbs the effect of multiple soft collisions and the tail accounts for the relatively rare hard collisions. The form used for the tail was

$$\left(\frac{df}{dT}\right)_e = \frac{1.042 A_0 B (T_0 - T)}{(T_0 - T)^3 + 2B^3} \quad , \quad A_0 = A_K \left(\frac{v_K}{v_0}\right)^2 \tag{3.2.3}$$

where T_0 and v_0 are the initial electron energy and speed and T is the energy when the electron reaches the active volume of the detector. The expression (3.2.3) is normalised so that the fraction of electrons in the tail is A_0 and the shifted peak correspondingly contained $1 - A_0$. The parameter A_K is a convenient measure of the amount of material, being the fraction of electrons in the tail of the ^{109}Cd K IC line, and the speed of undegraded ^{109}Cd K IC electrons is v_K. The form (3.2.3) varies inversely with the square of the speed of the incident electron and for $T' = T_0 - T \gg B$ also varies inversely with the square of

the energy lost in hard collisions. The tail peaks at $T' = B$ and this parameter represents some effective mean ionization potential, for in real material (3.2.1) must cut off at the ionization energy of the bound target electron. The value of B was found to be 0.2 keV, substantially less than the FWHM resolution. The ^{109}Cd K peak shifts were $\sim$ 0.1 keV at the beginning of a ^{35}S run and $\sim$ 0.2 keV at the end of a run — the difference arising through the build-up of a very thin layer of ice on the detector. The energy loss tail has a drastic effect on the measured β spectrum near the end point (section 5.1).

3.3 Back scattering component

The probability of normally incident electrons backscattering from the detector is $\sim$ 13.5% in the energy range 100–200 keV and does not change by more than 0.6% over this range [32,33]. The spectrum of energy T deposited in the detector peaks at $T/T_0 \sim 0.4$ and falls linearly to approximately zero probability at $T = T_0$ [32,12]. The form only departs significantly from linearity for $T/T_0 < 0.6$ and we did not fit outside this range. The functional form used for the effect of back scattering was

$$\left(\frac{df}{dT}\right)_b = \frac{S}{T_0}\left(1 - \frac{T}{T_0}\right) \quad , \quad \frac{T}{T_0} > 0.6 \tag{3.3.1}$$

which contains a fraction 0.035 above $T/T_0 = 0.6$, for the measured S of 0.44. The effect on the shape of the measured β spectrum is simple and gentle: at 105 keV the spectrum is depleted by a fraction 0.101, at 135 keV by 0.108 and at 165 keV by 0.110; a very shallow parabola. We modelled the form below $T/T_0 = 0.6$ only for the purpose of calculating sum pileup.

3.4 Flat component

We also added to the electron response function a component independent of the deposited energy

$$\left(\frac{df}{dT}\right)_F = \frac{F}{T_0} \quad , \quad T \leq T_0 \tag{3.4.1}$$

Such a term was included as part of the back scattering in [12], with the fraction $F = 0.015$. We treated F as a variable which could be adjusted to improve the fit to the ^{109}Cd IC tails and to remove residual long range curvature in the ^{35}S Kurie plot. In the latter case at least this term can absorb very efficiently the effect of more complicated long range tails such as might arise by scattering of electrons somewhere between the source and detector (section 5.2).

3.5 General features

The components (3.2.3), (3.3.1) and (3.4.1) of the electron response function are illustrated in fig.3.2 and were fitted to the ^{109}Cd IC spectra, after subtraction of background, over the range 30–88 keV. The data were well represented with the effective ionization potential $B = 0.2$ keV and the back scattering

slope $S = 0.44$. These values were used in all our final fits to both ^{109}Cd and ^{35}S.

The amount of flat component F was found to depend on the geometry and on the collimation, indicating the presence of an effect such as scattering, and varied between 1% and 4.5% for ^{109}Cd and between 2% and 6.5% when fitting ^{35}S. We would not expect the fractions of flat component to agree unless the physical effect represented by the flat component is both genuinely flat and the fraction energy independent (section 5.2).

3.6 Additional terms

When after run 8 we switched from an old ^{109}Cd source to a freshly prepared one, increasing the statistics from a single day of data by a factor ~ 10, we found that the fit was improved by an additional term in the energy loss component of the tail, with the same form as (3.2.3) but with a higher effective ionization potential $B' = 1.2\,\mathrm{keV}$. The fraction in the tail of the ^{109}Cd K line was $A'_K = 0.013$. This small effect was included in the response function for the analysis of all ^{35}S runs, but A'_K was not varied in the fits.

We also investigated the effect of adding terms of the form calculated for scattering from the original square cut baffle [17,34], peaking at $x = T/T_0 \sim 0.9$. Runs 6, 8 and 9 were made with a replica of the original square cut baffle and in run 9 the collimation and the source-detector geometry were the same as in run 2 of the original experiment [12]. The fit to the ^{109}Cd calibration data for run 9 was improved by the addition of a baffle scattering term of the form

$$\left(\frac{df}{dx}\right)_{bf} = \frac{1.042 f_B x_p x}{x^3 + 2x_p^3} \tag{3.6.1}$$

where the fraction f_B was 0.012 and x_p 0.91. (This form was suggested by (3.2.3) but a form proportional to $x^\gamma(1-x)$ — see section 5.2 — is very similar).

All ^{35}S runs were analysed without such a term. The effects of its inclusion for run 9 were studied separately (section 4.4).

4. Results.

4.1 Run details.

The duration, rate, detector and source numbers, source-detector distance, baffle and source collimator employed in each run are summarised in Table 4.1. Details of the baffles and source collimators are given in tables 4.2 and 4.3 respectively.

The square cut 0.8 mm aluminium baffle was a replica of that used in the original experiment [12]. This particular anti-scatter baffle is at least potentially a source of scattered electrons [17,34], for the flat cylindrical surface subtends a solid angle of ~ 0.05 steradians from the source and electrons scattered into the detector are under conditions of approximately specular reflection when the source is 56 mm from the detector. In this position the detector subtends ~ 0.03

steradians from the source. The knife edge baffle is a contrast; it presents no flat surface from which electrons could be scattered, with some energy loss, into the detector but at some level electrons must penetrate the edge and reach the detector as a result of scattering during passage through the aluminium. The chamfered baffle should in principle minimise both reflection from the interior conical surface and penetration of the edges of the aperture.

The composite baffle was designed to provide a different detector collimator by locating just in front of the normal aluminium collimator a copper one of smaller diameter. The copper was covered with perspex to reduce scattered electrons. This baffle was used with a wide open source collimator.

4.2 Analysis procedure.

Throughout these experiments the ^{35}S data were subjected to two independent analyses. In the first sequence, sum pileup was determined by fitting a parabola to the raw spectrum beyond the end point and subtracted from the data below the end point. The theoretical β spectrum was calculated from the simple analytic formula, with Coulomb corrections represented by a Gamow factor, which gives the intensity at the origin of an asymptotic outgoing plane wave. This spectrum was then corrected numerically for the effect of the measured pileup toe and finally multiplied by the product of shape factors to account for energy loss, back scattering, a flat component in the electron response function and the energy resolution. These shape factors were obtained by analytic convolution of a simple representation of the energy loss (eq.5.1.1) with a cutoff of 0.5 keV and of eqs.(3.3.1, 3.4.1) with the spectral form appropriate to the allowed β spectrum near the end point, $(Q-T)^2$. The effect of finite energy resolution was represented by convolution of a gaussian form. The slope of the back scattering was held fixed and the variables in the fit were normalisation, end point Q, an energy loss parameter P_K (eq.5.1.1) and the amount of flat component F (eq.3.4.1). Fits were made over the range 115–165 keV.

The second fitting sequence was more elaborate. First, a fully relativistic Fermi function was used, as in [12], but additional radiative corrections were not implemented because they make negligible difference [17]. As in [12], a screening potential of 1.73 keV was used. This spectrum was then convoluted numerically with the components of energy loss (sections 3.2, 3.6) to generate the spectrum corresponding to electrons passing through the source material and detector entrance layer. This was further convoluted numerically with the back scattering and flat components of the electron response function (sections 3.3, 3.4) and finally smeared with the gaussian resolution function (section 2.2). The resulting spectrum was used to calculate the sum pileup and the measured toe pileup was added. The final spectrum was fitted to the raw data over the range 100–200 keV. The parameters varied in the fit were normalisation, end point Q, energy loss parameter A_K (eq.3.2.3), amount of flat component F and the amount of sum pileup, largely determined by the spectrum beyond the end point. The amount of sum pileup increased a little faster than linearly with rate; the fitted resolving time of the pileup rejection unit increased linearly with rate from 330 ns at 2 kHz to 375 ns at 9 kHz. The slope of the back scattering component was held fixed at the value $S = 0.44$, as obtained from the ^{109}Cd calibration

and in agreement with both independent measurements [32] and Monte Carlo calculation [29]. (It was found that the slope S and the flat component F are inversely correlated in fitting to ^{35}S.)

The calculated sum pileup and the fit to the whole spectrum depends on the assumed shape of the electron response below $T/T_0 = 0.6$. The effect of altering this shape was investigated and found to have little effect on A_K (~ 0.02) and on the end-point ($\sim 0.02\,\mathrm{keV}$). The sum pileup was also calculated for some runs from the data themselves, as in [12], normalised beyond the end-point and then, together with the toe pileup, subtracted from the raw data. The results for A_K were very similar but with the values of A_K typically ~ 0.05 smaller and slightly dependent on the range used above the end-point in calculating the sum pileup; neither method of handling pileup is guaranteed to be absolutely correct and the corresponding uncertainty in A_K is estimated to be~ 0.03.

Excellent fits were achieved with both sets of programs. The magnitudes of the energy loss in the tail determined from the two sets were in good agreement, seldom differing by more than the statistical error. The same is true of the flat component and this agreement is reassuring. It should be emphasised that these excellent fits, with no 17 keV neutrino, were obtained only if the flat component, used to fit the long range curvature in the Kurie plot, and the energy loss were varied in the fit.

4.3 Results of fitting.

The final results which we present here are taken from the second sequence of fits described above. Fig.4.1 displays the residuals, in units of standard deviations, for the fits to all 14 runs under the assumption that there is no 17 keV neutrino. Table 4.4 lists for every run the mean energy loss parameter A_K and flat component as determined from the ^{109}Cd calibration runs. The next group of columns contains the results of fitting with no 17 keV neutrino, the energy loss parameter, flat component required, additional energy loss $\Delta A_K = A_K(^{35}\mathrm{S})$-$A_K(^{109}\mathrm{Cd})$, end point and the quality of the fit. The third group of columns gives the results of fitting with 0.8% of 17 keV neutrino imposed; in these fits the energy loss parameter A_K was constrained to be greater than or equal to the value obtained from the ^{109}Cd calibration data. The last columns contain the results of fitting with the admixture of 17 keV neutrino an additional free variable.

The fits with no 17 keV neutrino are in every case good. The fits with 0.8% 17 keV neutrino, with the energy loss constrained to be greater than or equal to that found from ^{109}Cd, are in almost every case bad and the energy loss is driven to the ^{109}Cd lower limit. The fits with the admixture free invariably converge on the fits with no 17 keV neutrino. There is no evidence whatsoever in these data for the existence of a 17 keV neutrino and subject to the proviso that there is no unknown systematic effect common to most runs the admixture determined from the 14 fits with $\sin^2\theta$ free

$$\sin^2\theta = -0.02\% \pm 0.05\%$$

corresponds to an upper limit of $\sin^2\theta < 0.1\%$ (95%CL).

The amounts of flat component vary significantly from run to run. The flat component determined from ^{35}S exceeds that determined from the corresponding ^{109}Cd data by 2% on average, although the two are not tightly correlated. It is noticeable that the amount of flat component when 0.8% of 17 keV neutrino is imposed is not much different from that with no 17 keV neutrino, implying that to the extent that the effects of scattering on the ^{35}S spectra can be modelled with a flat component in the electron response function (section 5.2), scattering effects were not primarily responsible for the results of [12].

The parameter $A_K(^{35}\mathrm{S})$ is typically twice $A_K(^{109}\mathrm{Cd})$; for source #2 the eleven individual determinations of ΔA_K are all consistent with the mean value. Since these runs were made with different geometries and collimation, this consistency gives us confidence that our modelling of long range effects in the electron response function is adequate. The rates varied from 2 kHz to 9 kHz and so the consistency also implies that the treatment of pileup is not seriously in error.

The mean value is

$$\Delta A_K = 0.48 \pm 0.03 \pm 0.05$$

where the first error is obtained from the variance and the second is our estimate of the effects of residual uncertainties in the treatment of pileup and in the modelling of the electron response function. The corresponding effective thickness of source #2 is $140 \pm 9 \pm 15\,\mu\mathrm{g\ cm}^{-2}$ if the source is composed of $BaSO_4$.

The data summarised in table 4.4 constitute very strong evidence that, first, there is no admixture of 17 keV neutrino at the level reported in [8,12] and secondly that ^{35}S electrons experience greater energy loss than the value extrapolated from ^{109}Cd electrons. It is not likely that, did a 17 keV neutrino exist at the 0.8% level, every run would reject it in favour of negligible admixture and increased energy loss.

The good null fits obtained are contingent on treating A_K and F as free parameters. The justification for treating A_K as a free parameter is first that, with the advantage of hindsight, there is no *a priori* reason to suppose that the strong $Ba^{35}SO_4$ sources are thin; secondly that these sources have been shown to be thick (section 6 and 7) although we have no very precise measure of the thickness. The flat component F, at the levels found to be required, should represent very well any long range effect which scales with fractional energy (section 5.2) and a flat component also gives good fits to the more demanding ^{109}Cd spectra. If the flat component must be fitted to the ^{109}Cd spectra, run by run, there is every reason to fit independently to ^{35}S; in the latter case the flat component, convoluted with the β spectrum, represents a convolution of some form which is probably more complicated (section 5.2).

If the energy loss is fixed at the value determined with ^{109}Cd, the residuals in fitting ^{35}S invariably exhibit a pronounced and characteristic kickup near the end point (see for example fig.2 of [27]), which is never eliminated by variation of the flat component. Such a kickup is characteristic of a 17 keV neutrino, but it is also characteristic of additional energy loss. The mechanism by which additional energy loss thus mimics a 17 keV neutrino was elucidated in [27] and is discussed in more detail in section 5.1.

4.4 Square cut baffles.

The original experiment [12] employed a square cut baffle under conditions of almost specular reflection. Piilonen and Abashian [17] calculate that under these conditions the square cut edge would deflect into the detector 2.6% of the electrons reaching the detector directly, with fractional energy peaking at ~ 0.95. Hime [34] finds $\sim 1.5\%$, peaking at 0.92–0.93. These levels of scattering would be represented by $\sim 10\%$ and 5% of flat respectively, when fitting to ^{35}S (section 5.2) but the peaked form might be resolved in ^{109}Cd[34]. Since the publication of [27] we have measured directly the effects of scattering from the square cut baffle. Our results (section 5.3) are closer to those in [34] than [17].

We investigated the effect of such a peaked form of baffle scattering with a re-analysis of the data of run 9, which duplicated run 2 of [12] (except in rate), with a square cut baffle, 5 mm source collimator and source-detector distance 56 mm. A new ^{109}Cd source had been prepared before run 9 and the calibration spectrum is statistically strong. This spectrum was reasonably well fitted without any peaked scattering term, but better fitted when such a term was added. The ^{109}Cd response function was best represented with the addition of a 1.2% tail peaked at a fractional energy of 0.91. The results are summarised in table 4.5 and illustrated in fig.4.2.

When the peaked term, with parameters determined from^{109}Cd, was included in the electron response function for fitting ^{35}S, the principal result was that the flat component decreased by the amount expected. The effect on the fitted value of ΔA_K was marginal, a decrease of 0.13.

Run 9 was taken under conditions as near as possible to those of the original experiment and it is interesting to see how evidence for a heavy neutrino goes away step by step (table 4.6). Fits were made with a variable amount of heavy neutrino under increasingly more realistic assumptions, starting with no pileup toe, no peaked scattering term and energy loss fixed at the value extracted from the ^{109}Cd calibration.

The peaked baffle scattering term is largely interchangeable with flat — both affect primarily the long range curvature of the Kurie plot and have relatively little effect on the kickup near the end point. Allowance for scattering through either variable flat or a peaked term improves the quality of fits but does not play a major role in destroying the distortion near the end point. This distortion pulls in an admixture of heavy neutrino, of mass ~ 17 keV, which is not destroyed until the energy loss is allowed to increase.

We note that Piilonen and Abashian [17] concluded that the effects of scattering from the baffle, aperture penetration and back diffusion from the source modify but do not destroy the serious distortion in the data of [12]. Hime [34] showed that changing the electron response function to allow for these effects yielded a χ^2 for the hypothesis of no 17 keV neutrino equal to that obtained with a 17 keV neutrino when using the original response function. It would have been better to have fitted with the new response function and the neutrino admixture free, for the truncated residuals in figs.4(a),(b) of [34] suggest that the kickup has by no means been eliminated, as in fact noted by Hime.

4.5 A limit insensitive to the electron response function.

All fourteen runs together contain $\sim 10^7$ events keV^{-1} in the region of 150 keV and with these statistics it was feasible to search a restricted energy range for a heavy neutrino kink. All fourteen runs had been taken with almost identical dispersion and were summed with offsets chosen to align the 150 keV points. (The biggest such offset was six channels, 0.465 keV.) The summed data were rebinned in groups of thirty two channels (2.48 keV) and the second differences proved to be linear, with no trace of a heavy neutrino signature, over the range 136–164 keV. The data were well fitted by a third order polynomial (regardless of whether or not the background due to pileup was subtracted), but this was not true if the range was extended further towards the endpoint. Fitting with a third order polynomial multiplied by the shape factor for a 17 keV neutrino we found

$$\sin^2\theta = 0.05\% \pm 0.065\%$$

or $\sin^2\theta < 0.18\%$ (95%CL).

This result did not depend significantly on the number of channels in a group (groups of twelve and of thirty two channels were used), nor on shifts of the grouping relative to the channels. The same procedure applied to the more restricted range 140–160 keV yielded a limit of 0.25%. In fig.4.3 we show the data divided by the best fits for $\sin^2\theta = 0$ (a) and 0.7% (b), the variables in the fit being the four polynomial coefficients. The range was 136–164 keV and the bins groups of twelve channels. The results of this study do not depend on the assumed form of the electron response function and are insensitive to any possible systematic effects, because any such effects would be smooth.

5. Residual shape factor

When a recorded β spectrum is fitted with an imperfect model the best fit will deviate systematically from the data. The fractional difference is the residual shape factor and we discuss below the forms generated by the short range effect of energy loss and effects which control the long range curvature of the Kurie plot.

5.1 Effect of energy loss on the residual shape factor

The principal effects of energy loss on β spectra near the end point emerge from a very simple model. The probability that an electron of kinetic energy T loses energy T' in a single collision is taken as

$$\frac{dP(T,T')}{dT'} = \frac{P_K}{T}\frac{1}{T'^2} \qquad \left(B \le T' \le \frac{T}{2}\right) \tag{5.1.1}$$

The effect of energy loss on a β spectrum of form $f(T)$ is then $(T > Q/2)$

$$f(T) \to f_{EL}(T) = \left(1 - \frac{P_K}{BT}\right) f(T) + \int_{T+B}^{Q} \frac{P_K}{T_1}\frac{dT_1}{(T_1 - T)^2} f(T_1) \tag{5.1.2}$$

(The integral is easily evaluated for the approximation $f(T) = (Q-T)^2$ but the resulting expression is complicated and the qualitative features only emerge when the function is plotted.) The shape factor associated with energy loss is

$$S_{EL}(T) = f_{EL}(T)/f(T) \tag{5.1.3}$$

The cutoff B represents a mean ionization potential and is less than the energy resolution: bins within B of the end point are depleted by a fraction P_K/BT, which under the conditions of these experiments is ~ 0.2. Lower bins are similarly depleted, but also fed by the second term in (5.1.2). Because the probability (5.1.1) is inversely proportional to the square of the energy lost, the effect is short range and the second term rapidly compensates; 5 keV below the end point the depletion is only ~ 0.1 and it drops smoothly to ~ 0.05 17 keV below the end point and to $0.025 \sim 60\,\mathrm{keV}$ below the end point.

Because the shape factor associated with energy loss turns down sharply near the end point, one would suppose that fitting a β spectrum in the presence of additional unsuspected energy loss would generate a kickdown in the residual shape factor near the end point. Were the value of the end point Q kept fixed, a kickdown would of course be obtained but the end point is never sufficiently well known and must be allowed to vary in the fit, as pointed out by Simpson and Hime [8]. Shifting the end point to obtain the best fit overcompensates for the kickdown and generates a kickup of the kind observed. The origin of the effect is easily understood in terms of a simple analytic argument.

The shape factor associated with energy loss is quite well represented by the simple form

$$S_{EL} = 1 - \frac{a}{\sqrt{Q-T}} \qquad (Q - T > 1 \text{ keV}) \tag{5.1.4}$$

In the region of the end point the β spectrum with energy loss is of the form

$$(Q-T)^2 \left\{ 1 - \frac{a}{\sqrt{Q-T}} \right\}$$

and if a represents an unsuspected energy loss, this is fitted with a form $(1-\alpha)(Q+\epsilon-T)^2$, where α and ϵ are parameters to be varied in the fit. Variation of α corresponds to varying the normalisation or effective activity of the source and ϵ is the difference between the end point in the fit and the true end point. Setting $x = Q - T$, the difference between the actual and fitted spectra is $x^2(1 - ax^{-1/2}) - (1-\alpha)(x+\epsilon)^2$ so that

$$\chi^2 = \sum_i \frac{N^2[x_i^2(1 - ax_i^{-1/2}) - (1-\alpha)(x_i+\epsilon)^2]^2}{Nx_i^2} \tag{5.1.5}$$

where N is a normalisation constant and the error in each bin has been taken as $\sqrt{Nx_i^2}$. The best fit is achieved by minimising χ^2 with respect to α and ϵ simultaneously. Replacing the sum by an integral over x we achieve an analytic χ^2 minimisation. To first order in small quantities the best fit is given by

$$\frac{\partial \chi^{2\prime}}{\partial \alpha} = 0 \quad , \quad \frac{\partial \chi^{2\prime}}{\partial \epsilon} = 0$$

where

$$\chi^{2\prime} = \int_0^{x_0} [-ax^{1/2} - 2\epsilon + \alpha x]^2 dx \tag{5.1.6}$$

This yields

$$\alpha = \frac{4}{5} a x_0^{-1/2}$$

$$\epsilon = -\frac{2}{15} a x_0^{1/2}$$

and the residual shape factor is

$$RS = -ax^{-1/2} + \alpha - 2\epsilon x^{-1}$$

which is the difference between the shape factors associated with energy loss $S_{EL} = 1 - ax^{-1/2}$ and with a shift in the end point $S_Q = 1 - \alpha + 2\epsilon x^{-1}$. With the substitution of the best fit values of α and ϵ

$$RS = -ax^{-1/2} + \frac{4}{5} a x_0^{-1/2} + \frac{4}{15} a \frac{x_0^{1/2}}{x} \tag{5.1.7}$$

The last term is responsible for the kickup in RS as the end point is approached ($x \to 0$). To first order in small quantities the shape of RS is independent of the energy loss parameter a and the magnitude varies linearly with a. The shape factors S_{EL} (5.1.4) and S_Q, the latter corresponding to the best fit assuming no unknown energy loss, were plotted in fig.3 of [27], the residual shape factor (5.1.7) in fig. 4a of [27]. The limit on integration was $x_0 = 47\,\mathrm{keV}$, corresponding to fitting ^{35}S from 120 keV to very close to the end point. The energy loss parameter was $a = 0.1\,\mathrm{keV}^{1/2}$, corresponding to an unsuspected energy loss equivalent to $P_K \sim 6\,\mathrm{keV}^2$ or $A_K \sim 0.5$. The fitted parameters were $\alpha = 0.0117$ and $\epsilon = -0.091\,\mathrm{keV}$.

Rather than repeat those figures, we have computed residual shape factors by generating ^{35}S β spectra and fitting the generated spectra with the more precise fitting program used in the analysis of the data. The results are presented in fig.5.1.

Figs.5.1a,b show the residual shape factor for a β spectrum generated with $A_K = 1.0$, no 17 keV neutrino and a flat component $F = 0.05$, fitted by varying normalisation and end point but assuming $A_K = 0.5$ and $F = 0.05$. This corresponds to an unsuspected ΔA_K of 0.5. In fig.5.1a the fit is from 100 keV and in fig.5.1b from 120 keV. Figs.5.1c,d show the residual shape factor which would be due to 0.5% 17 keV neutrino admixture; the generated spectrum was characterised by $A_K = 0.5$, $\sin^2\theta = 0.005$ and $F = 0.05$. It was fitted by varying normalisation and end point, assuming $A_K = 0.5$, $\sin^2\theta = 0.00$ and $F = 0.05$. Finally, figs.5.1e,f show the residual shape factor due to 5% flat component in the electron response function. The generated spectrum was characterised by $A_K = 1.0$, $F = 0.05$ and it was fitted assuming $A_K = 1.0$, $F = 0.00$. The form of the residual shape factor induced by a flat component is discussed in the next section.

Comparison of figs.5.1a,b with fig.5.1c,d respectively shows that the residual shape factors for energy loss and for a 17 keV neutrino are remarkably similar.

The two factors differ most in the range 145 keV–155 keV, where the neutrino residual shape factor exhibits the notorious kink. In this region the errors on individual bins are, for a single run, similar to or greater than the differences in this region. In a single run it is impossible to assert or deny the existence of a kink at $\sim$ 150 keV, but in our data every run is better fitted by increased energy loss than by a significant admixture of 17 keV neutrino. When the data from all fourteen runs are combined the spectrum is very smooth between 136 and 164 keV and a 17 keV neutrino kink is excluded, $\sin^2\theta < 0.18\%$ (95% CL).

Comparison of fig.5.1b,d with fig.4a,b of [27] shows that the present calculations differ from the analytic calculation in [27]. Below $\sim$ 140 keV the energy loss shape factor fig.5.1b clings close to the axis, whereas in fig.4a of [27] there is a distinct slope. The present calculation resembles the shape factor for a 17 keV neutrino even better than that in fig.4a of [27]. The reason is that the approximate representation of the energy loss shape factor (5.1.4) is sufficient to demonstrate the origin of the kickup in the residual shape factor, but is not sufficiently accurate at the level of a few tenths of a percent. The shape factor for energy loss is better represented by the form

$$1 - a(x)x^{-1/2}$$

where $a(x) = a_0 - a_1 x + a_2 x^2$ with a_i positive numbers. When the parameters a_i are chosen to match the calculated shape factor for energy loss more precisely, an analytic χ^2 minimisation indeed reproduces the features exhibited in figs.5.1a,b.

The shapes of (5.1.7) and figs.5.1(a,b) are largely independent of the amount of energy loss (which enters (5.1.7) as a single multiplicative parameter). Thus any significant amount of unsuspected energy loss can be misinterpreted as evidence for a neutrino of mass $\sim$ 17 keV, the fitted admixture being proportional to the amount of unsuspected material.

5.2 Long range effects

We modelled long range effects by a fixed back scattering component, to which was added a variable flat component. If some effect, such as scattering from an intermediate aperture, adds a fraction F of electrons from an individual bin at kinetic energy T and distributes them uniformly between 0 and T, the effect is

$$f(T) \rightarrow f_F(T) = f(T) + \int_T^Q \frac{F}{T_1} f(T_1) dT_1 \qquad (5.2.1)$$

The shape factor S_F is very simple if $f(T)$ is set equal to $(Q-T)^2$, as appropriate for an allowed β transition near the end point, and to first order in $x = Q - T$ takes the form

$$S_F = 1 + \frac{F}{3}\frac{x}{Q} \qquad (5.2.2)$$

The effect of fitting with an allowed β spectrum, the end point varying, in the presence of an unknown amount of flat component is easily calculated; the residual shape factor is

$$RS = \frac{F}{3Q}\left\{x - x_0 + \frac{1}{6}\frac{x_0^2}{x}\right\} \qquad (5.2.3)$$

The numerically calculated residual shape factor is plotted in figs.5.1e,f for an unknown amount of flat component $F = 0.05$ (the difference between flat in ^{35}S and ^{109}Cd fitting seldom exceeds half this value).

Comparison of fig.5.1e with figs.5.1a,c and fig.5.1f with figs.5.1b,d show that the residual shape factors for energy loss, a 17 keV neutrino and a flat component in the response function all exhibit a kickup near the end point, a term proportional to x^{-1} which dominates at small x. Such a term will almost invariably arise as a result of shifting the end point — if the spectrum fitted is modified by a shape factor $1 - s(x)$ then the residual shape factor takes the form

$$-s(x) + \alpha - 2\epsilon x^{-1}$$

where α and ϵ have the best fitted values.

It is obvious that the residual shape factor due to a flat component is very different from that due to either a 17 keV neutrino or additional energy loss when the fit is performed from 100 keV. The difference is less pronounced when the fit is performed from 120 keV. Starting the fit further down is an advantage in discriminating between long range effects such as scattering and short range effects such as energy loss — or a 17 keV neutrino.

The representation of scattering effects by the addition of a flat component may at first sight seem both arbitrary and implausible, but any long range tail in the electron response function yields much the same effect. Suppose that the tail takes the form

$$x^{\gamma}(1 - x) \tag{5.2.4}$$

where $x = T/T_0$ and a scattered electron with initial kinetic energy T_0 reaches the detector with energy T. This form with $\gamma \gtrsim 9$ represents quite well the form of the scattering from a baffle as calculated by Hime [34] and is easily convoluted with the $(Q - T)^2$ end of the β spectrum. The corresponding shape factors are very smooth and approximately linear, quite unlike the shape factor associated with energy loss, which plunges dramatically as the end point is approached. Thus 4% flat component augments the β spectrum by 0.8% at 100 keV and by 0.4% at 130 keV (and not at all at the end point). If (5.2.4) is employed, with $\gamma = 9$ which peaks the scattered spectrum at 0.9, then 4% scattering augments the β spectrum by 2.3% at 100 keV and by 1.1% at 130 keV; in fits to the β spectrum, 4% flat could well represent $\sim 1.4\%$ peaked scattering with $\gamma = 9$, or similarly $\sim 0.9\%$ scattering with $\gamma = 19$, for which the scattered electrons peak at $x = 0.95$. Fig.5.2 shows the residual shape factors corresponding to 5% flat and to 2% of a form peaking at $x = 0.91$. Both are simple smooth curves, quite unlike short range effects. The ^{109}Cd spectra are of course more sensitive to the detailed form of the scattered distribution, but with the exception of one of the runs with a square cut baffle acquired with high statistics did not require any addition of the form (5.2.4).

Other effects which will distort the β spectrum at some level are back diffusion from the source substrate and penetration of the edges of apertures. The energy dependence and form of the distribution in energy of the degraded electrons has been calculated for the configuration of the original experiment [17,34]. The two sets of calculations agree in the energy dependence and in the

distribution of degraded energy, but differ substantially in absolute magnitude. The forms of the shape factors corresponding to these calculations are easily estimated by folding with the spectral form $(Q-T)^2$ and both effects induce a long range curvature in the Kurie plot which can be quite well represented by a flat component in the electron response function. We find, for example, that if the tail due to aperture penetration contains 1% of the direct electrons at 167 keV, this is equivalent to a flat component containing $\sim 2\%$.

We are confident that, within the statistical accuracy of our runs, long range effects such as intermediate scattering, back diffusion from the source and aperture penetration can be subsumed within a variable flat component in the electron response function. It is however clear that one cannot expect a perfect correspondence between the proportion of flat needed to fit ^{109}Cd and that found in fitting the ^{35}S spectra.

5.3 Measurements of scattering from baffles

Since the publication of [27] we have measured the contribution of scattering from the square cut and knife edge baffles, with the source 56 mm from the detector. The measurements were made with electrons from the ^{109}Cd IC lines, with direct electrons screened out, and the spectrum due to scattering from a single baffle obtained from the differences between the spectra recorded with different numbers of identical baffles. The scattered spectra were well measured above ~ 23 keV.

Scattering into the detector from the square cut baffle peaks at a fractional energy of 0.93 but is not well represented by a single term of form (5.2.4), nor by the calculations of [17,34] — the low energy tail is too high. The data are well represented by the sum of two terms of form (5.2.4), the first peaking at a fractional energy of 0.93, containing 1% of direct IC electrons, and the second peaking at 0.76 and containing 0.6% of direct electrons. The shape is very well measured near the energy of the IC lines and there is no discrete interval between the primary line and the highest energy scattered electrons. This measurement directly contradicts the inference of a gap of ~ 20 keV drawn in [25].

The effect of scattering from the very different knife edge baffle proved to be negligible, at ^{109}Cd IC energies. However, in contrast to scattering from a flat surface, the effect of scattering in penetration of a knife edge is expected to grow approximately linearly with the range of the incident electrons in the material.

6. Investigation of the presence of additional energy loss

It being established that the kickup in the ^{35}S shape factor is eliminated by allowing the energy loss to increase, there remained a number of possibilities. The first is that the energy loss as determined from ^{109}Cd IC lines is appropriate for the ^{35}S data and that the 17 keV neutrino exists. This is implausible because additional energy loss is preferred to a significant admixture of 17 keV neutrino in all fourteen runs (and because of the negative results from a number of careful independent experiments). The second is that some effect, such as scattering

or aperture penetration, is mimicking additional energy loss. We investigated this possibility to some extent by adding a right angled triangle to the electron response function, with apex at full energy and base reaching to a fraction x_c of the full energy. The kickup is satisfactorily reproduced for x_c in the range 0.92–0.98, with the triangular term containing $\sim$ 2% of the electrons at the lower limit and $\sim$ 20% at the upper. Such an effect is short range, much more localised than the calculations of scattering, back diffusion from the source and aperture penetration reported in [17,34]. It therefore seemed likely that additional energy loss was indeed present but to be sure it was necessary to find the origin. Knowing that a significant amount of ice built up on the detector in the course of all runs, one possibility was that ice accumulates on the source as well as on the detector. This we eliminated in two ways. First, the detector was not warmed up between runs 5 and 6, but the ^{35}S source was removed and spent several days at room temperature before reinstallation. During the first of these two runs the broad peak at low energy, which is induced in the β spectrum by energy loss, moved steadily upwards as the run progressed. The upward march during run 6 matched the extrapolation from run 5; there was no discontinuity. Secondly, a long run was made with a ^{109}Cd source. When a substantial amount of ice had accumulated, as measured by the downward shift of ^{109}Cd Auger L lines, the source was removed, warmed and reinserted. The Auger L lines did not move.

The only other possibility that occurred to us was that the $BaSO_4$ sources, prepared by chemical deposition, were in fact clumped and thick — a few tenths of a μm. Sources deposited **as hydroxides** have been shown to be thin [28] but D. Wark had found that merely adding a solution of $Ba(NO_3)_2$ to a drop of distilled water deposited on a source substrate resulted in clumps of barium, in association with both sulphur and silicon [35]. These measurements had been made with Proton Induced X-ray Emission (PIXE), using the Oxford Proton Microprobe [36], and the clumps had local area density in excess of 40 μg cm^{-2} of barium.

6.1 Tilting the source

We first investigated the possibility that the $BaSO_4$ sources are locally thick by mounting source #2 at 45° to the normal orientation. The position of the peak of the β spectrum was found to be at $\sim$ channel 170 after one day. On returning the source to the usual orientation, 0°, the peak was found to be at $\sim$ channel 135. We had already calibrated approximately the shift of the β spectrum peak against the change in energy loss as measured with ^{109}Cd sources at the beginning and end of runs; a shift of 35 channels (2.7 keV) was known to correspond to a change in the energy loss parameter A_K of $\sim$0.23, if entirely due to additional material passed through by the electrons. The implication was that source #2 material presents $\Delta A_K \sim 0.57$ to electrons reaching the detector. (With the more careful calibration discussed in section 6.4 the shift of 35 channels corresponds to a change in A_K of 0.18, or $\Delta A_K = 0.43$.) The value of ΔA_K thus inferred was roughly equal to the additional thickness needed to account for the shape factor of the ^{35}S β spectrum over the last few keV.

This could not be regarded as settling the matter, because of the possibility that effects other than energy loss cause a shift in the low energy peak of the β spectrum when the geometry is changed by tilting the source. We compared ^{109}Cd spectra taken at 0° and 45° and found that while the positions of the IC and Auger L peaks did not change on tilting the source, the long range tail below the IC peaks was augmented by an additional few per cent of the peak intensity when the source was tilted. We embarked on three further investigations.

6.2 Proton microprobe studies of source #1

Source #1 being at that time 8 half lives old, we cut a disc from the centre and glued it to a target holder which was mounted in the beam of the Oxford Proton Microprobe [36]. The microprobe beam is $\sim 1\,\mu$m across and the thickness and composition of a sample can be investigated by Proton Induced X-ray Emission (PIXE) and by Rutherford Back Scattering (RBS) of the microprobe beam.

A coarse scan of an area $2.5 \times 2.5\,\mathrm{mm}^2$ yielded a mean area density of $34\,\mathrm{ng\ cm}^{-2}$ of barium, as determined from the yield of barium L X-rays. This is a factor ~ 3 greater than would be expected from the initial source activity, were all the barium deposited in association with ^{35}S. Fine scans of a number of areas $100\,\mu$m square revealed local concentrations of barium. These were associated with calcium, silicon, sulphur and chlorine, as mapped with PIXE, and were sufficiently thick to screen out gold M X-rays from the source substrate. In sixteen $100\,\mu$m squares, three such concentrations were found. The first consisted of two adjacent areas of diameter $\sim 12\,\mu$m and PIXE spot checks yielded 15, $40\,\mu\mathrm{g\ cm}^{-2}$ of barium, with similar amounts of silicon and calcium. (Sulphur can be difficult to detect because the sulphur K line lies close to gold M). RBS indicated total thicknesses of $\sim$ 125, $250\,\mu\mathrm{g\ cm}^{-2}$ of mixed barium and calcium sulphates and silicates. The second concentration consisted of three adjacent areas each of diameter $\sim 12\,\mu$m. PIXE spot checks yielded 30, $68\,\mu\mathrm{g\ cm}^{-2}$ of barium, with relatively little silicon or calcium. RBS indicated total thicknesses of 72, $124\,\mu\mathrm{g\ cm}^{-2}$, mostly barium sulphate. The third concentration had dimensions $\sim 30\,\mu\mathrm{m} \times 40\,\mu$m and was both thick and inhomogeneous. It proved too complex to extract absolute numbers from PIXE, but from the relative proportions and from RBS it was concluded that it is probably thicker than $\sim 400\,\mu\mathrm{g\ cm}^{-2}$ and an inhomogeneous mixture of barium and calcium sulphates and silicates.

These results can only be indicative, for in the time available less than 1% of the active source was scanned with sufficient resolution to detect concentrations with dimensions $\sim 10\,\mu$m. However, it is clear that it is not safe to assume that the sulphur sources are locally thin and it is not safe to assume the composition of the source layer to be predominantly barium sulphate. These observations alone justify varying A_K in fitting ^{35}S.

6.3 Source tilting with ^{109}Cd

We investigated systematically the origin of the additional long range tail in the response to ^{109}Cd electrons, which had appeared on tilting the source

from 0° to 45°. The possibilities seemed to be either additional scattering or increased back diffusion from the source backing at 45°. We measured the tails in the response function at 0°, 34° and 40° and found that major changes in collimation did not significantly affect the additional tails. We then added an inert source foil behind that carrying the ^{109}Cd source. Addition of a foil at 0° increased the fraction of electrons in the tails of the IC lines by ~ 0.05 of the line intensity and addition of a foil at 40° by ~ 0.11. We took this as evidence that back diffusion from the source is significant at ~ 60 keV and that the increased tail observed on tilting the ^{109}Cd source is to be attributed to increased back diffusion.

Below ~ 20 keV back diffusion from the source foil alone must be at saturation and a change in the amount or shape of saturated back diffusion could affect the position of the β spectrum peak, even in the absence of additional energy loss. We could not measure saturated back diffusion at such low energies, but repeated the 0° and 40° ^{109}Cd measurements with a 1 mm thick plastic disc placed directly behind the source substrate, in order to measure saturated back diffusion of the IC lines. If there were no back diffusion from the source alone, subtraction of the source spectrum from the normalised spectrum of the source backed by the plastic disc would yield a superposition of saturated back diffusion from the K, L and M IC lines of ^{109}Cd. The back diffusion from the source alone is unknown (and will not be represented by the difference between the foil backed source and the bare source); the best we could do was to fit differences. We assumed that each line contributed to the difference spectrum a fraction a with a shape given by the form $x(1-x)^\gamma$, where x is the fractional energy of the back diffusing electron and the parameters a and γ were to be fitted. The peak of the back diffused spectrum x_p is related to γ by

$$\gamma = \frac{1}{x_p} - 1.$$

Fits were made over regions excluding the IC lines themselves and excluding the low energy region containing X-rays and Auger electrons. The results are summarised in table 6.1.

One would expect that an increase of the amount of back diffusion, without change of shape, would result in a downward shift of the β spectrum peak. An increase in the peak of the back diffusion, without changing the proportion of back diffused electrons, would be expected to shift the β peak upwards. The shape of the saturation back diffusion does not change dramatically as the source is tilted — the peak position increases and at the same time the amount of back diffusion increases. The two effects will tend to compensate in the shift of the β spectrum peak.

We note that tilting the ^{109}Cd source never resulted in a detectable displacement of the IC or Auger full energy peaks. This is consistent with the ^{109}Cd source being thin but we can only set a limit of $\Delta A_K \leq 0.1$, a thickness $\lesssim 30\,\mu$g cm^{-2}.

6.4 Determination of thickness by tilting ^{35}S sources

We obtained an estimate of the effect of the change in back diffusion with a simple model. We supposed that low energy electrons are smeared by energy loss into a spectrum of the form

$$\frac{dN}{dx} \propto x^n e^{-x} \tag{6.4.1}$$

with $x = \lambda \Delta T$, where ΔT is the energy lost. The parameters n and λ were chosen such that the most probable energy loss and the mean energy loss were given by the Landau distribution [37]. With the β spectrum modified by this representation of energy loss and the addition of back diffusion the qualitative features of the upward shift of the peak with increasing A_K were reproduced (but the model required rather more increase of energy loss for a given β peak shift than we have measured). Changing the characteristics of back diffusion from those determined (for 60 keV electrons) at 0° to those at 40° resulted in a shift upwards in the peak of less than 1 channel, for fixed energy loss.

The peak shift of $\sim$ 35 channels observed when source #2 was tilted through 45° is, in the light of the ^{109}Cd studies, unlikely to be due to scattering. The change in back diffusion seems too small to be of much significance. There remained the probability that source #2 was locally thick and we therefore attempted to make a thin source using a technique similar to that described in [22].

Source #3 was prepared by first evaporating 10 nm of barium metal on a standard backing foil, 100Å of gold on $\sim$ 3 μm of mylar. A drop of $Na_2{}^{35}SO_4$ solution was placed on the layer of barium and allowed to evaporate. Soluble residues were then removed by two three minute washes. We had hoped that bringing the $Na_2{}^{35}SO_4$ into intimate contact with a thin evaporated layer of barium would result in a far more uniform deposit of $Ba^{35}SO_4$ than obtained by precipitation with $Ba(NO_3)_2$ and hence a locally thin source, but #3 proved to be only $\sim$ 20% thinner than #2.

We carried out a systematic programme of comparisons of the β peak positions with sources #2 and #3, at source angles of both 0° and 40°. An eight day run with source #3 followed, after which we made further comparisons of #2 and #3, at both angles, with a significant coating of ice on the detector. It was immediately obvious that #3 was thinner than #2, for the β peak position at the beginning of a run with source #3 was as low as channel 104 (8 keV) whereas with #2 the peak was never seen below channel 135 (10.4 keV). (Source #1 had been observed to peak as low as channel 108). The results of our measurements of the β spectrum peak shifts are summarised in table 6.2 and an example is shown in fig.6.1.

The relation between the β spectrum peak shifts and the change in the energy loss parameter A_K responsible was determined empirically from the runs with source #2 and the single run with source #3. At the beginning and end of each ^{35}S run ^{109}Cd spectra were taken, from which initial and final values of A_K were extracted. The ^{35}S data were read out daily and so the position of the low energy peak at the end of the first and last days of ^{35}S data could be determined. The only assumption necessary in establishing the calibration is that ice

buildup on the detector occurred at a uniform rate. The quantity $20\Delta A_K/\Delta n$ is displayed in fig.6.2 as a function of $\bar{n}$, where ΔA_K is the interpolated change of A_K during a ^{35}S run, Δn is the number of channels by which the β peak shifted and $\bar{n}$ is the mean of the peak channel numbers at the end of the first and last days of ^{35}S data.

The calibration data below channel 180 are obviously well represented by a straight line of positive slope; a greater increment in energy loss is necessary to produce a given peak shift as the mean energy loss increases. This empirical feature (which is also found in our attempt to model the process) is very important in the interpretation of the data in table 6.2. Beyond channel 180 there are only two points, the last being relatively poorly determined. The reason for this paucity of data is simply that we seldom made ^{35}S runs with a lot of ice on the detector. The figure shows three fits to the calibration data, summarised in table 6.3. The first is a straight line fit to only those points with $\bar{n} < 190$. The second is a straight line fit to all points and the third a parabolic fit to all points. The general form is

$$20\frac{\Delta A_K}{\Delta n} = a_0 + a_1\bar{n} + a_2\bar{n}^2. \tag{6.4.2}$$

The data in table 6.2 show one very clear qualitative feature. The larger the mean value of the peak position $\bar{n}$, the smaller the shift Δn for a given change of source or configuration. The calibration studies make it clear that this is a signature of an energy loss mechanism.

The data not only suffice to determine the thickness of source #2 and of source #3, but these parameters are overdetermined. We define the effective thickness of a source to be the average path length in source material of electrons emitted approximately normal to the plane of the source; fitting to the data of table 6.2 yields these effective thicknesses, t_2 and t_3, directly in terms of the energy loss parameter A_K.

We do not know whether a straight line or a parabola is the truer calibration and the data are not sufficient to determine the form. We also do not know directly the features of saturation back diffusion at low energies, $\lesssim 20\,\mathrm{keV}$. We therefore made a number of fits to the data of table 6.2, in terms of variables t_2, the difference $t_2 - t_3$ and a third parameter c which represented the peak shift due to the change in back diffusion on tilting the source. The peak shift due to increased energy loss was taken to be the measured shift Δn when comparing different sources in the same orientation but

$$\Delta n - c(1 + 0.005(\bar{n} - 150))$$

when comparing different orientations. (The small change with $\bar{n}$ in the shift due to back diffusion was indicated by our model of the process). Fits were made using all three calibration curves and with c as a free parameter as well as fixed at zero (as suggested by the model). The results are summarised in table 6.4. (We also fitted the calibration and shift data simultaneously but this made no significant difference.)

It is clear that if the parabolic calibration is correct, then $t_2 \sim 0.3$ with c free, whereas the straight line fits prefer $t_2 \sim 0.35$. If c is fixed at zero then

$t_2 \sim 0.43$. The difference between t_2 and t_3 is very well determined and almost independent of assumptions. We concluded that

$$t_2 = 0.35 \pm 0.05 \pm 0.05$$
$$t_2 - t_3 = 0.093 \pm 0.007 \pm 0.002$$
$$c = 6 \pm 3 \pm 4$$

where the thicknesses are given in units of A_K, the first error is statistical and the second an estimate of the effects of uncertainty in back diffusion and in calibration beyond channel 180. The disparate data in table 6.2 are well fitted and internally consistent with energy loss in thick sources. (The above value of t_2 corresponds to $102 \pm 15 \pm 15\,\mu$g cm^{-2} of $BaSO_4$). These studies of the shift in position of the low energy peak of the β spectrum have demonstrated that source #2 is certainly more than half as thick as inferred from the other end of the β spectrum and the thickness extracted is consistent with that inferred from the distortion near the end point, $\Delta A_K = 0.48 \pm 0.03 \pm 0.05$, provided only that the shift due to changes in back diffusion is small, as we expect.

At this point in our work we had three pieces of evidence that energy loss in the source is responsible for the kickup at the end of the β spectrum, originally attributed to a heavy neutrino. First, the data in all fourteen runs were fitted better with extra energy loss than with a significant admixture of 17 keV neutrino. Secondly, the microprobe studies of source #1 showed clumps of source material of about the right thickness and thirdly source tilting revealed directly that the sources are about the right thickness. We then followed a suggestion of A. Hime [29] and looked for barium K X-rays excited by electrons passing through the source material. We predicted that if the effective thickness of material passed through by electrons reaching the detector from source #2 is equivalent to $\sim 100\,\mu$g cm^{-2} of $BaSO_4$, then $\sim 10^5$ barium K X-rays should be clearly visible in the total of 86 days of source #2 ^{35}S data (but the signal would not be detectable in any individual run). We found them.

7. Studies of characteristic X-rays from the source

The electron flux from the decay of ^{35}S ionizes atoms in the source material and in the source substrate. We have detected barium K_α X-rays in the summed source #2 runs at a level which corresponds to an average path length in barium $\sim 100\,\mu$g cm^{-2} and this constitutes **conclusive** evidence that source #2 is locally thick. As a control we have studied gold $L_{\alpha,\beta}$ X-rays from the source substrate, which are present at a level which corresponds to an average path length in gold of $\sim 35\,\mu$g cm^{-2}; the nominal perpendicular thickness of the evaporated gold layer is $20.7\,\mu$g cm^{-2}. (In both cases the average is taken over all decay electrons.) We have also searched for barium L X-rays. We have not identified a clear signal, but the upper limit is not inconsistent with the barium K_α signal.

7.1 Yield of barium K X-rays as a measure of source thickness.

The eleven runs of source #2 comprise 86 days of data taking, $\sim 460\,\mathrm{kHz}$ days of electrons in the detector. The runs have almost identical dispersion and the spectra were summed, after allowing for a small change in the zero offset which occurred when a ground was installed. The bins were then combined in groups of four, because the ADC exhibits a systematic stagger every fourth channel at the 0.1% level. Each group of four contained $\sim 1.1 \times 10^8$ counts, in the region of the barium K X-rays.

The barium K_α signal is too small to be visible in the raw data, but is very clear in the residuals to a straight line fit (fig.7.1.a). These data were fitted locally with a second order background, to which was added a term with the barium K_α profile. The difference between the data and the second order background is shown in fig.7.1.b, together with the fitted signal. The fit is good, $\chi^2/dof = 14.7/21$, and the fitted number of barium K_α X-rays is $(1.19 \pm 0.23) \times 10^5$, for $\sim 4 \times 10^{10}$ electrons in the detector.

The source aperture is the same for both electrons and the X-rays and so the number of X-rays N_{X_i} detected in the same solid angle as the electrons is related to the number of electrons N_β by

$$N_{X_i} = \langle \sigma_i \rangle \frac{\bar{t}_i}{M_i} \omega_i \epsilon_i N_\beta \tag{7.1.1}$$

where $\langle \sigma_i \rangle$ is the cross section for ionization of the appropriate atomic level, averaged over the ^{35}S β spectrum. The mean distance travelled by decay electrons in material of atomic mass M_i is $\bar{t}_i$, in units of mass per unit area. The quantity ω_i is the X-ray fluorescent yield and ϵ_i the efficiency of the detector for the full energy peak.

The cross section for ionization of inner shells by electrons is frequently represented by the Bethe formula [38]

$$\sigma_{n\ell} = \pi e^4 \frac{Z_{n\ell} b_{n\ell}}{B_{n\ell}} \frac{1}{T} \ln\left(\frac{c_{n\ell} T}{B_{n\ell}}\right) \tag{7.1.2}$$

where T is the electron kinetic energy and $B_{n\ell}$ the ionization energy of the shell with quantum numbers (n, ℓ). The quantity $Z_{n\ell}$ is the number of electrons in the shell. This formula is usually used at relatively high energies, $T/B_{n\ell} > 4$ and popular values of the parameters $b_{n\ell}$, $c_{n\ell}$ are unlikely to be appropriate at low energies. We are not aware of data on barium K shell ionization by electrons near threshold and have determined values of $b_{n\ell}$ and $c_{n\ell}$ by comparison of eq.(7.1.2) with extensive low energy data on the ionization of the silver K shell [39]. The choice $c_K = 1$ ensures that (7.1.2) goes smoothly to zero at threshold and with $b_K = 0.95$ the silver data are well represented between threshold and $T/B_K \sim 4$, corresponding to the range 37 to $\sim 150\,\mathrm{keV}$ for barium. With these choices for c_K and b_K we find, on averaging over the ^{35}S β spectrum $\langle \sigma_K \rangle_{Ba} = 1.4 \times 10^{-23}$ cm^2. The fluorescent yield of barium K_α X-rays is 0.73 [40] and the photoelectric absorption cross section for 32 keV X-rays is 0.9 cm^2 g^{-1}; the efficiency of a 5 mm thick silicon detector is ~ 0.65. The aluminium

detector collimator transmits ~ 0.6 of 32 keV X-rays and we estimate that of 1.19×10^5 detected barium K_α X-rays $(0.4 \pm 0.2) \times 10^5$ were detected outside the area accessible to electrons†. We therefore take for the value of $N_{X_{Ba}}$ in (7.1.1) $(0.8 \pm 0.15 \pm 0.2) \times 10^5$ and (7.1.1) then yields an average path length in barium $\bar{t}_{Ba}$ of $70 \pm 13 \pm 17\,\mu g\ cm^{-2}$ from the summed source #2 data. This corresponds to an average path length $\bar{t}_{BaSO_4}$ of $119 \pm 22 \pm 29\,\mu g\ cm^{-2}$ if all the barium precipitated as the sulphate.

7.2 The relation between average path length and effective thickness.

The energy lost in the source material by electrons reaching the detector is determined by the effective thickness, denoted by t (section 6.4). The yield of X-rays is determined by the path length averaged over all electrons, which are emitted isotropically. This average path length is denoted by $\bar{t}$. The relation between the two depends on the unknown detailed topography of the clumped source material.

The effective thickness of a clump is the average path length traversed by those electrons reaching the detector, which leave the source approximately perpendicular to the plane. If ^{35}S is distributed homogeneously throughout the precipitated material, the effective thickness t_c is half the thickness of the clump, defined by the mass or volume of the clump divided by the area covered. This we denote by τ_c. We express the average path length in the clump in terms of τ_c.

If a clump takes the form of a crystal for which the diameter of the base is approximately equal to the height, it is obvious that the average path length $\bar{t}_c$ is approximately half the thickness τ_c and that the effective thickness t_c is approximately equal to the average path length $\bar{t}_c$. Thus if the source were composed of such crystals, widely separated, the effective thickness t of the source, which determines energy loss, would be approximately equal to the average path length, $\bar{t}$, which determines X-ray yield.

At the other extreme, suppose the locally thick patches of source material take the form of flat plates. Electrons directed more or less perpendicular to the plates go straight through; electrons directed very obliquely to the normal will either leave through an edge or be scattered out of a flat face. In the notation of fig.7.2 the amount of material passed through is approximately r, provided that $r \leq r_c$ where r_c is a cutoff parameter. Since $r = \tau_c / \cos\theta$ and an element of solid angle is $2\pi d \cos\theta$, then for the case shown in fig.7.2 the average path length $\bar{t}_c$ is given by

$$\begin{aligned} \bar{t}_c &= \frac{1}{2}\left\{ \tau_c \int_{\tau_c/r_c}^{1} \frac{d\cos\theta}{\cos\theta} + r_c \int_0^{\tau_c/r_c} d\cos\theta \right\} \\ &= \frac{\tau_c}{2}\left\{ 1 + \ln\left(\frac{r_c}{\tau_c}\right) \right\} \end{aligned} \tag{7.2.1}$$

† This effect was overlooked in [27].

and hence since $t_c \simeq \tau_c/2$

$$t_c \simeq \frac{\bar{t}_c}{1 + \ln\left(\frac{r_c}{\tau_c}\right)}$$

If $r_c \sim \tau_c$, then the effective thickness t_c is approximately equal to the average path length $\bar{t}_c$, as expected. The cutoff distance r_c has to be several times the thickness τ_c before the effective thickness t_c falls to half the average path length.

We take as a reasonable criterion for evaluating the limit r_c that imposed by multiple scattering

$$\frac{\theta_s^2}{6} r_c^3 = \frac{\tau_c^2}{4} \tag{7.2.2}$$

where the left hand side is the mean square displacement perpendicular to the original line of flight, projected on one plane, after a distance r_c [41]. The multiple scattering parameter θ_s is given by

$$\theta_s^2 = \left(\frac{E_s}{p\beta c}\right)^2 \frac{1}{X_0} \tag{7.2.3}$$

where $E_s = 21\,\mathrm{MeV}$, X_0 is the radiation length of the material and $p\beta c$ is approximately twice the kinetic energy of the low energy electron. Then

$$\frac{r_c}{\tau_c} = \left(\frac{X_0}{\tau_c}\right)^{\frac{1}{3}} \left(\frac{3}{2}\right)^{\frac{1}{3}} \left(\frac{2T}{E_s}\right)^{\frac{2}{3}} \tag{7.2.4}$$

The radiation length in $BaSO_4$ is $12\,\mathrm{g\ cm^{-2}}$ and for this material

$$\frac{r_c}{\tau_c} = \tau_c^{-\frac{1}{3}} 0.56 T^{\frac{2}{3}}$$

where τ_c is measured in $\mu\mathrm{g\ cm^{-2}}$ and T in keV. If $\tau_c \sim 200\,\mu\mathrm{g\ cm^{-2}}$ then r_c/τ_c varies from 1.1 at 40 keV to 2.7 at 150 keV. It is reasonable to conclude from (7.2.1) that if $\bar{t}_{BaSO_4}$ is $119\,\mu\mathrm{g\ cm^{-2}}$ then

$$71\,\mu\mathrm{g\ cm^{-2}} < t_{BaSO_4} < 119\,\mu\mathrm{g\ cm^{-2}}.$$

Thus the yield of barium K_α X-rays implies an effective thickness

$$t_{BaSO_4} = 95 \pm 18 \pm 23 \pm 29\,\mu\mathrm{g\ cm^{-2}}$$

where the first error is statistical, the second represents the uncertainty in the number of X-rays detected outside the area accessible to electrons and the third represents the uncertainty caused by lack of knowledge of the detailed topography of the source. Adding all three in quadrature

$$t_{BaSO_4} = 95 \pm 40\,\mu\mathrm{g\ cm^{-2}}$$

The effective thickness t_{BaSO_4} required to fit near the end point of the ^{35}S β spectrum is $140 \pm 9 \pm 15\,\mu\mathrm{g\ cm^{-2}}$. If calcium salts are also present the required thickness of barium salts is of course reduced.

7.3 Yield of gold $L_{\alpha,\beta}$ X-rays

The sources are deposited on a gold layer of nominal thickness 20.7 μg cm^{-2}, evaporated on a mylar backing 2–3 μm thick. In the early stages of the experiment we observed very clean gold $L_{\alpha,\beta}$ signals (at 9.7 and 11.5 keV) in a one day run of source #1, screened by 0.0125 g cm^{-2} of aluminium. We found 3253 ± 304 gold $L_{\alpha,\beta}$ X-rays, which after correction for absorption in the screen becomes 4485 ± 420 gold L X-rays in an exposure equivalent to 2.1 kHz days. Gold L X-rays are also clearly visible in the summed source #2 data. There are approximately 10^6 with an uncertainty on this number of $\sim 0.25 \times 10^6$, completely dominated by uncertainties in the form of the background under the signal, for an exposure of 460 kHz days. These two measurements are entirely consistent and correspond to ~ 2150 gold L X-rays/kHz day.

The cross section for the yield of gold L X-rays has been measured above 60 keV [42] and the ionization cross sections of the gold L shells [42,43] agree with the calculations in [44]. We chose $c_L = 1$ and the product $b_L\bar{\omega}_L$ so as to match the measured cross sections for gold L X-rays at 60 keV. With these choices

$$\{\langle\sigma_L\rangle\bar{\omega}_L\}_{Au} = 2.3 \times 10^{-22}\,\mathrm{cm}^2$$

The average cross section is much more uncertain than that for the barium K shell, because 60% is contributed by electrons between threshold and 60 keV, where there are no suitable data. The quoted errors on the measured cross sections at 60 keV are $\sim 8\%$ and it seems unlikely that the cross section we have used is wrong by more than 30% below 60 keV. We therefore assign an uncertainty of $\pm 4.5 \times 10^{-23}$ cm^2 to the cross section for the production of gold L X-rays. The detected yields then correspond to average path lengths of gold of $36 \pm 4 \pm 7\,\mu$g cm^{-2} for the screened source #1 run and $38 \pm 9 \pm 8\,\mu$g cm^{-2} for source #2.

The nominal thickness of the gold substrate is 20.7 μg cm^{-2} and the criterion of eq.(7.2.4) yields $r_c/\tau \sim 2$. For a uniform layer eq.(7.2.1) leads us to expect an average path length $\bar{t} \simeq 20\,\mu$g cm^{-2}. The effect of electrons scattered back into the gold from the mylar support might add $\sim 5\,\mu$g cm^{-2}. There is thus some discrepancy between the number of gold L X-rays actually detected and our estimates of the cross section and average path length in the gold layer. The gold layer is unlikely to be uniform, but non-uniformity need not increase $\bar{t}$.

7.4 Search for barium L X-rays

Barium L X-rays would present a blended profile with a peak at 4.5 keV. This region is not accessible under the conditions used for taking ^{35}S data and barium L X-rays were searched for early on, in a 2.2 kHz day exposure of source #1 with the gain increased by a factor ~ 10. Fig.7.3 shows the environment of the barium L region, between 0 and 12 keV. The blended barium L signal would lie almost at the bottom of a deep and asymmetric trough, between the very steeply falling noise and the low energy rise of the β spectrum. (It is not possible to screen out the electrons without also screening out low energy X-rays.) The only striking feature is the strong chlorine K_α line at 2.62 keV. This can only be

due to autoionization in the β decay of ^{35}S. The line contains $\sim 6 \times 10^4$ counts, which corresponds to

$$P_K \bar{\omega}_K \simeq 3 \times 10^{-4}$$

where P_K is the probability of K shell autoionization and $\bar{\omega}_K$ the mean fluorescent yield, which is 0.094 [40]. The calculations of [45] give for the probability of a K shell vacancy following β decay of ^{35}S $P_K = 3.9 \times 10^{-3}$ and these calculations are in good agreement with such autoionization probabilities as have been measured. The identity of the line at 2.62 keV is certain. Aluminium K_α is present, sulphur K_α and gold M would lie on the low side of chlorine K_α and a chlorine K_β line would be expected at 2.82 keV, with only 8% of the K_α intensity. Any calcium K_α would occur at $\sim$ 3.8 keV. On the far side of the trough, copper K_α and gold L_α X-rays are barely visible.

There is a slight bulge in the silt at the bottom of the trough at 4.5 keV, which might be a barium L X-ray signal. A fit over the range 3–7.7 keV to the barium L profile, with a second order background, yielded $(1.24 \pm 0.23) \times 10^4$ barium L X-rays, but in view of the lack of precise knowledge of the form of the background we cannot exclude with confidence any number between 0 and 2×10^4 barium L X-rays.

The average path length in barium in source #2, as determined with barium K_α X-rays, is $\sim 70\,\mu$g cm^{-2}. Source #1 is 20% thinner and so the average path length in barium is expected to be $\sim 60\,\mu$g cm^{-2}. In the absence of data on the low energy cross section for barium L shell ionization, we chose $c_L = 1$ and $b_L = 0.9$, for which eq.(7.1.2) matches the calculations of [44] for barium L shells at 50 keV. It is far from clear that eq.(7.1.2), with these parameters, will be valid down to threshold at 5.5 keV; two thirds of the estimated mean cross section

$$\langle \sigma_L \rangle_{Ba} = 3.5 \times 10^{-21} \text{cm}^2$$

is due to electrons below 50 keV. The fluorescent yield $\bar{\omega}_L$ is 0.09 [46] and for an exposure of 2.2 kHz days we expect $\sim 1.6 \times 10^4$ barium L X-rays. The data in the environs of barium L are not inconsistent with source #1 having an average path length $\sim 60\,\mu$g cm^{-2} of barium.

7.5 Searches for barium X-rays in the original data

Subsequent to [12] A. Hime looked for barium K X-rays [29] in data from the second run of the original experiment, 33 kHz days. He found no signal and claimed a limit on the source thickness of $15\,\mu$g cm^{-2}, with an expected yield of 1.8×10^5 barium K X-rays for a source thickness of $250\,\mu$g cm^{-2} of $BaSO_4$, an estimate which we have been unable to reproduce. For those conditions we calculate a yield of only $\sim 1.5 \times 10^4$ barium K X-rays and such a signal would not be detectable above the β spectrum background. Hime also looked for barium L X-rays in the residuals to a parabolic fit between 3 and 7 keV, from a one day run with increased gain. He found none and claimed a limit of $\sim 10\,\mu$g cm^{-2}. We have been unable to detect with any certainty barium L X-rays from a source where the local surface density is $\sim 200\,\mu$g cm^{-2}. We conclude that Hime's failure to detect barium X-rays from the source used in the original experiment cannot be taken as evidence that it was locally thin.

8. Conclusions.

Our exhaustive investigations of the β spectrum of ^{35}S have revealed no evidence whatsoever for the existence of a 17 keV neutrino and have uncovered the origin of the undoubtedly spurious signal reported in [12]. We have worked throughout with essentially the same apparatus and techniques as described in [12] and [29] and have discovered

(i) A pileup toe unsuspected in the work of [12]

(ii) A component in the long range tail of the electron response function which varies with geometry and collimation; this component induces long range curvature in the Kurie plot. It cannot be determined with sufficient accuracy from calibration IC electrons but must be included in the β spectra fits.

(iii) That $Ba^{35}SO_4$ sources are clumped and locally thick ($\sim 200\mu g\ cm^{-2}$) so that energy loss in the source is about equal to that in the contact and dead layer of the detector.

The data of [12] were analysed with a predetermined electron response function and in particular it was assumed that energy loss could be extrapolated from results obtained with ^{109}Cd and ^{57}Co IC lines. If our data are analysed under this assumption, they exhibit the characteristic kickup near the end point which was in [12] interpreted as evidence for a 17 keV neutrino. The positive result reported in [12] must have been due predominantly to energy loss in the source, with some contribution from scattered electrons and the pileup toe.

The weakest statement we can make is that in the light of our results neither [8] nor [12] can be taken as positive evidence for a 17 keV neutrino. Our own results in fact set a stringent limit; combining all 14 runs we find

$$\sin^2\theta = -0.02\% \pm 0.05\%$$

where the error is taken from the variance of the 14 results. This variance must contain the effects of some systematic fluctuations and if there is no significant systematic effect common to the majority of our runs, our result corresponds to the limit

$$\sin^2\theta < 0.1\% \quad (95\%\text{CL}).$$

In the analysis leading to this stringent limit the energy loss component of the electron response function was varied to achieve the best fit. This is justified by the measures of source thickness we have obtained from barium K X-rays and by tilting the source and those measurements are entirely consistent with the mean source thickness inferred from the ^{35}S spectrum near the end point. It might be that our modelling of the electron response function is somehow inadequate, inducing a false preference for additional energy loss as opposed to a 17 keV neutrino signal (but we doubt it). Against such a possibility, we can set ΔA_K equal to the **minimum** value indicated by the barium X-ray and source tilting results, which we take to be 0.3 for source #2 (and consequently 0.2 for sources #1 and #3). The effect would be to increase $\sin^2\theta$ by $\sim 0.2\%$, with an upper limit

$$\sin^2\theta < 0.3\%.$$

This is overly conservative because the model independent search for a kink in the combined data yielded a limit

$$\sin^2\theta < 0.18\% \qquad (95\%\text{CL}).$$

We find the end point of the ^{35}S β spectrum to be $Q = 167.60 \pm 0.03\,\text{keV}$, where the error is taken from the variance of the 14 individual results in table 4.4†. We estimate that possible common systematic errors in calibration and treatment of pileup introduce an additional uncertainty of $\pm 0.04\,\text{keV}$. Combining these errors in quadrature yields $Q = 167.60 \pm 0.05\,\text{keV}$.

It would seem that the two recent experiments on ^{35}S with silicon detectors were successful in avoiding potential and actual problems of the kind which plagued [8,12] and the present work. Both used magnetic fields to transport the electrons, which encountered no material between source and detector. The magnetic field snared half the electrons in the single detector experiment [24], an effective solid angle of $\sim 2\pi$, and in the double detector experiment the effective solid angle was $\sim 4\pi$. The sources were therefore very weak; according to [24] $\sim 0.1\mu$Ci over an area of diameter 1.5 mm on $20\mu\text{g cm}^{-2}$ carbon foil, with an initial counting rate $\sim 3\,\text{kHz}$. In the double detector experiment [25] a source of 0.5 mm diameter and activity $\sim 0.03\mu$Ci was deposited on a $5\mu\text{g cm}^{-2}$ carbon foil, giving an initial count rate $\sim 1\,\text{kHz}$. In both cases these weak sources were made by evaporation of droplets of $Na_2{}^{35}SO_4$ solution deposited on the foils. It is claimed in [24] that the average thickness of the $Na_2{}^{35}SO_4$ residue was less than $0.1\,\text{ng cm}^{-2}$ and the authors of [25] claim that the energy loss within the source does not surpass several tens of electron volts, on the basis of measurements made on IC sources prepared by drying droplets of radioactive HCl solutions on to carbon foils. We are not aware of any direct evidence that the sources used in [24,25] were indeed locally thin, but the extreme weakness permitted and required by the magnetic collimation seems in favour and in neither case did the fits assuming thin sources require any admixture of 17 keV neutrino!

With the demolition of [12], we doubt that [8] can be taken as positive evidence for a 17 keV neutrino. The remaining β experiments yielding positive results for a 17 keV neutrino are a measurement of the ^{63}Ni β spectrum [29] with the apparatus of [12], a measurement of the ^{14}C β spectrum with ^{14}C dissolved in germanium [13] and the two experiments with tritium implanted in solid state detectors [1,11]. In the ^{63}Ni experiment discussed in [29] the source was deposited as the hydroxide, but the apparent 17 keV signal is very vulnerable to smooth correction factors which could arise from intermediate scattering and from back diffusion from the source. According to the calculations in [34] the 17 keV signal vanishes when these effects are included in the electron response function. The original analysis which showed evidence for a 17 keV neutrino admixture in the ^{14}C β spectrum [13] has been invalidated by recent studies of the instrumental response [47]. We note finally that in addition to the negative results from β spectra summarised in table 1.1 the absence of any

† This differs from the value given in [27] because of a small error in calibration found subsequently. This error is otherwise of no significance.

kink corresponding to a 17 keV neutrino in the ^{55}Fe internal bremmstrahlung spectrum has been convincingly demonstrated [47,48]; the 95% CL upper limit on a 17 keV neutrino admixture is quoted as 0.14%. (It was this work which inspired us to search for a kink in our combined data). The origin of the very low energy distortion in the tritium spectra [1,11] is as yet unexplained, but the 17 keV neutrino is dead.

D.H. Perkins made valuable contributions in the early stages of this work. The proton microprobe studies of source #1 were made by G.W. Grime and in the measurements of baffle scattering we had the assistance of A. Tomlinson. We thank D. Wark for a number of useful conversations and in particular for drawing our attention to evidence that $BaSO_4$ sources prepared by chemical deposition could be locally thick.

References

[1] J.J. Simpson, *Phys. Rev. Lett.* **54** (1985) 1891

[2] T. Altizoglou *et al*, *Phys. Rev. Lett.* **55** (1985) 799

[3] A. Apalikov *et al*, *JETP Lett.* **42** (1985) 289

[4] J. Markey and F. Boehm, *Phys. Rev.* **C32** (1985) 2215

[5] V.M. Datar *et al*, *Nature* **318** (1985) 547

[6] T. Ohi *et al*, *Phys. Lett.* **B160** (1985) 322

[7] J.J. Simpson in Proc. XXIth Rencontre de Moriond, VIth Workshop. Massive neutrinos in Astrophysics and in Particle Physics. O. Fackler and J. Tran Thanh Van, eds. Editions Frontieres, Gif-sur-Yvette 1986 p565

[8] J.J. Simpson and A. Hime, *Phys. Rev.* **D39** (1989) 1825

[9] G. Bonvicini, *Z. Phys.* **A345** (1993) 97

[10] D.W. Heatherington *et al*, *Phys. Rev.* **C36** (1987) 1504

[11] A. Hime and J.J. Simpson, *Phys. Rev.* **D39** (1989) 1837

[12] A. Hime and N.A. Jelley, *Phys. Lett.* **B257** (1991) 441

[13] B. Sur *et al*, *Phys. Rev. Lett.* **66** (1991) 2444

[14] Proc. XXVIth Rencontre de Moriond, XIth Workshop. Massive neutrinos Tests of fundamental symmetries O. Fackler, G. Fontaine, J. Tran Thanh Van, eds. Editions Frontieres, Gif-sur-Yvette 1991
Proc. Joint International Lepton-Photon Symposium and Europhysics Conference on High Energy Physics 1991. S. Hegarty, K. Potter and E. Quercigh, eds. World Scientific Singapore 1991
Workshop on the 17 keV neutrino question, Berkeley December 1991

[15] A. Hime *et al*, *Phys. Lett.* **B260** (1991) 381
G. Gelmini, S. Nussinov and R.D. Peccei, *Int. J. Mod. Phys.* **A7** (1992) 3141 and references therein.

[16] D.R.O. Morrison in Proc. XXVIIth Rencontre de Moriond, XIIth Workshop. Progress in Atomic Physics Neutrinos and Gravitation. G. Chardin, O. Fackler, J. Tran Thanh Van, eds. Editions Frontieres, Gif-sur-Yvette 1992 p207

[17] L. Piilonen and A. Abashian in Proc. XXVIIth Rencontre de Moriond, XIIth Workshop. Progress in Atomic Physics Neutrinos and Gravitation. G. Chardin, O. Fackler and J. Tran Thanh Van, eds. Editions Frontieres, Gif-sur Yvette 1992 p225

[18] H. Kawakami *et al*, *Phys. Lett.* **B287** (1992) 45
T. Oshima *et al*, *Phys. Rev.* **D47** (1993) 4840

[19] *Nuclear Physics* **B** (Proc. Suppl.) **31** (1993)

[20] Proc. XXVIIIth Rencontre de Moriond, XIIIth Workshop. Perspectives in Neutrinos Atomic Physics and Gravitation. J. Tran Thanh Van, T. Damour, E. Hinds and J. Wilkerson, eds. Editions Frontieres, Gif-sur-Yvette 1993

[21] E. Holzschuh and W. Kündig in Proc. XXVIIIth Rencontre de Moriond, XIIIth Workshop. Perspectives in Neutrinos Atomic Physics and Gravitation. J. Tran Thanh Van, T. Damour, E. Hinds and J. Wilkerson, eds. Editions Frontieres, Gif-sur-Yvette 1993 p329

[22] M. Chen *et al*, *Phys. Rev. Lett.* **69** (1992) 3151

[23] G.E. Berman *et al*, *Phys. Rev.* **C48** (1993) R1

[24] J.L. Mortara *et al*, *Phys. Rev. Lett.* **70** (1993) 394

[25] H. Abele *et al*, *Phys. Lett.* **B316** (1993) 26

[26] D.O. Caldwell, invited talk, 1992 Meeting of the Division of Particles and Fields, American Physical Society, Batavia IL (1992)

[27] M.G. Bowler and N.A. Jelley, *Phys. Lett.* **B331** (1994) 193

[28] H.A. Wyllie and G.C. Lowenthal, *Int. J. Appl. Radiat. Isot.* **35** (1984) 257

[29] A. Hime, D.Phil. Thesis, Oxford 1991 (unpublished) OUNP–91–20

[30] A. Hime, private communication.

[31] B. Planskoy, *Nucl. Instr. Methods* **61** (1968) 285

[32] A. Damkjaer, *Nucl. Instr. Methods* **200** (1982) 377

[33] T. Tabata *et al*, *Nucl. Instr. Methods* **94** (1971) 509

[34] A. Hime, *Phys. Lett.* **B299** (1993) 165

[35] D. Wark, private communication

[36] G.W. Grime *et al*, *Nucl. Instr. Methods* **B54** (1991) 52

[37] K. Siegbahn (ed), *Alpha, beta and gamma spectroscopy Vol I* North Holland, Amsterdam 1966 p13

[38] C.J. Powell, *Rev. Mod. Phys.* **48** (1976) 33

[39] D.V. Davis *et al*, *Phys. Lett.* **38A** (1972) 169

[40] C.M. Lederer and V.S. Shirley, eds. Table of Isotopes (7th ed.) Wiley, New York 1978

[41] B. Rossi, *High Energy Particles* Prentice-Hall, N.J. 1952

[42] J. Palinkas and B. Schlenk, *Z. Phys.* **A297** (1980) 29

[43] S. Reusch *et al*, *Z. Phys.* **D3** (1986) 379

[44] J.H. Schofield, *Phys. Rev.* **A18** (1978) 963

[45] J. Law and J.L. Campbell, *Phys. Rev.* **C12** (1975) 984

[46] W. Bambynek *et al*, *Rev. Mod. Phys.* **44** (1972) 716

[47] F.E. Wietfeldt, LBL-35568 (1994)

[48] F.E. Wietfeldt *et al*, *Phys. Rev. Lett.* **70** (1993) 1759

Table 1.1

Source	**Technique**	$\sin^2\theta$	**end point (keV)**	**Ref.**
^{63}Ni	Magnetic spectrometer	$(-0.11 \pm 0.33 \pm 0.30) \times 10^{-3}$ $< 0.73 \times 10^{-3}$ 95%CL	$66.9459 \pm 0.0044 \pm 0.0032$	[18]
^{63}Ni	Magnetic spectrometer	$(0.37 \pm 0.55) \times 10^{-3}$	66.9655 ± 0.0059	[21]
^{35}S	Magnetic spectrometer	$(-0.5 \pm 1.4) \times 10^{-3}$ $< 2 \times 10^{-3}$ 90%CL	167.55 ± 0.04	[22]
^{35}S	Magnetic spectrometer	$(0.1 \pm 1.5) \times 10^{-3}$	$167.228 \pm 0.009 \pm 0.1$	[23]
^{35}S	Solid state detector magnetic collimation	$(-0.4 \pm 0.8 \pm 0.8) \times 10^{-3}$	$167.27 \pm 0.005 \pm 0.100$	[24]
^{35}S	Solid state detector magnetic collimation	$< 1.9 \times 10^{-3}$ 90%CL	167.35	[25]
^{35}S	Solid state detector metal collimators	$(-0.2 \pm 0.5) \times 10^{-3}$	167.60 ± 0.05	This work

Table 4.1

Run Data

Run #	Duration (days)	Rate (kHz)	Detector	Source #	Source-Detector Distance (mm)	Baffle	Source Collimator
1	12	2.3	1	1	56	knife edge	5 mm
2	12	2.0	1	1	56	knife edge	5 mm
3	8	6.8	2	2	112	knife edge	5 mm
4	8	6.4	2	2	112	knife edge	5 mm
5	7	8.9	2	2	56	knife edge	3 mm
6	7	6.4	2	2	56	square cut	3 mm
7	8	5.2	2	2	84	knife edge	5 mm
8	8	4.5	2	2	84	square cut	5 mm
9	8	6.2	2	2	56	square cut	5 mm
10	8	5.0	2	2	56	knife edge	5 mm
11	8	4.4	2	2	56	chamfered	5 mm
12	8	3.7	2	2	56	knife edge	5 mm
13	8	2.0	2	2	61	composite	15 mm
14	8	3.0	2	3	56	knife edge	8 mm

Table 4.2

Baffles

	Material	**Minimum diameter**	**Chamfer**	**Distance from detector**
Knife edge	0.8 mm Al	31 mm	67° fs	32 mm
Square cut	0.8 mm Al	26 mm	square cut	32 mm
Chamfered	0.8 mm Al	26 mm	40° fd	32 mm
Composite	Perspex, Cu	6 mm	30° fd	16 mm

fs, fd refer to larger apertures facing source and detector respectively.

Table 4.3

Source Collimators

Minimum diameter	Material	Chamfer	Distance from Source
3 mm	1 mm Cu	10° fs	4 mm
5 mm	1 mm Cu	10° fs	4 mm
8 mm	1 mm Cu	12° fs	4 mm
15 mm	1 mm Cu	30° fs	4 mm

fs signifies the large aperture facing the source

Table 4.4

Results of fitting ^{35}S spectra over the range 100–200 keV. The parameters A_K and F extracted from ^{109}Cd calibration are shown on the left. In all the fits summarised, A_K, F, Q, the amount of sum pileup and the normalisation were varied.

	^{109}Cd		^{35}S										
			no heavy neutrino					**0.8% 17 keV ν**		**variable A_K and % 17 keV ν**			
Run	A_K	F%	A_K	F%	ΔA_K	Q	χ^2 (156 dof)	F%	χ^2 (156 dof)	A_K	F%	$\sin^2\theta$(%)	χ^2 (155 dof)
1	0.50	2.2	0.79	1.8	0.29	167.709	141	1.9	180	0.91	1.8	−0.19	141
2	0.40	2.8	0.80	1.7	0.40	167.826	124	1.9	144	0.80	1.7	0.00	124
3	0.60	2.1	0.96	5.8	0.36	167.453	137	6.1	182	0.95	5.8	0.00	137
4	0.42	4.0	0.83	6.6	0.41	167.509	168	6.7	213	0.90	6.5	−0.11	167
5	0.50	2.5	1.04	4.7	0.54	167.526	166	4.8	200	0.99	4.7	+0.07	166
6	0.94	4.6	1.26	3.7	0.32	167.442	158	3.7	228	1.49	3.8	−0.27	154
7	0.42	0.9	0.90	4.2	0.48	167.562	160	4.4	184	0.85	4.3	+0.07	160
8	0.40	1.8	0.89	5.9	0.49	167.564	162	6.0	182	0.82	5.9	+0.09	162
9	0.40	3.5	1.06	6.3	0.66	167.717	147	6.5	159	0.86	6.3	+0.25	144
10	0.59	1.2	1.16	3.7	0.57	167.646	163	3.8	175	0.99	3.7	+0.22	161
11	0.41	2.1	0.90	4.5	0.49	167.607	171	4.7	209	1.08	4.4	−0.23	169
12	0.41	1.9	0.86	4.1	0.45	167.578	166	4.2	196	0.99	4.0	−0.18	165
13	0.43	2.5	0.91	6.0	0.48	167.598	153	6.2	157	0.81	6.0	+0.14	152
14	0.42	1.6	0.72	5.9	0.30	167.646	149	6.0	172	0.78	5.9	−0.10	148

The statistical errors on $A_K(^{109}\mathrm{Cd})$ are < 0.002 and on $F(^{109}\mathrm{Cd}) < 0.15\%$. The statistical error on $F(^{35}\mathrm{S})$ is $\sim 0.2\%$. The statistical errors on $A_K(^{35}\mathrm{S})$ were in the range 0.09–0.11 and on Q 29–34 eV. The statistical errors on $\sin^2\theta$ (last group of columns) ranged from 0.13–0.21%. Where averaged values of the last three quantities are quoted, values from each run were given equal weight.

Table 4.5

Effects of adding a peaked baffle scattering term when fitting the run 9 ^{109}Cd calibration spectrum.

	No peaked term	**Peaked term fitted**
Position of peak (fractional energy)	—	0.91
Fraction in peaked term	0	0.012
A_K	0.399	0.397
F (%)	3.5	1.9
χ^2/dof	22750/723	17100/721

Table 4.6

Successive fits to the data of run 9

Fit	ΔA_K	**Pileup toe (%)**	**Scatt %**	**Flat %**	$\sin^2\theta$ (%)	**Mass (keV)**	χ^2/dof
1	0	0	0	6.9	0	–	245/157
2	0	0	0	6.8	0.75	17.3	172/155
3	0	0.72	0	6.5	0.61	17.4	155/155
4	0	0.72	1.2	3.7	0.55	17.0	149/155
5	0.48	0.72	1.2	3.4	0.15	16.7	147/155
6	0.48	0.72	1.2	3.4	0	–	150/157

Underlined quantities were not varied in the fits. Fits 1 and 2 show that neglect of additional energy loss and the pileup toe generates an apparently robust 17 keV neutrino signal. This signal is reduced by the inclusion of the measured pileup toe (0.72%), fit 3. The effect of including 1.2% of a scattering term peaked at fractional energy 0.91, as determined from ^{109}Cd (Table 4.5), is slight. It is only when additional energy loss is included that the apparent evidence for a 17 keV neutrino vanishes. (The additional energy loss in fits 5 and 6 is the mean from all source #2 runs).

Table 6.1

Fits to the difference between plastic disc backed ^{109}Cd spectra and source alone. DS denotes disc backed spectra and S source alone

Spectra	a	x_p
DS(0°)-S(0°)	0.175	0.38
DS(40°)-S(0°)	0.28	0.62

Table 6.2

The shifts in the low energy peak of the ^{35}S spectrum between different sources and configurations are tabulated as a function of mean peak position. The first section gives shifts determined by the difference in thickness between sources #2 and #3; the second gives shifts determined by the increase in thickness perceived by electrons reaching the detector when sources are tilted.

Measurement	**Change of thickness**	$\bar{n}$	Δn
Measurements of peak shifts between sources			
0°	$t_2 - t_3$	130	29 ± 4
40°	$1.305(t_2 - t_3)$	152	24 ± 3
0°	$t_2 - t_3$	163	16 ± 3
0°	$t_2 - t_3$	200	14 ± 4
40°	$1.305(t_2 - t_3)$	218	10 ± 4
Measurements of peak shifts on tilting sources			
40° – 0°	$0.305t_3$	130	30 ± 4
40° – 0°	$0.305t_3$	192	22 ± 3
40° – 0°	$0.305t_2$	152	25 ± 3
45° – 0°	$0.414t_2$	154	34 ± 3
40° – 0°	$0.305t_2$	220	18 ± 3

Table 6.3

Parameters obtained fitting calibration data to the form

$$20\frac{\Delta A_K}{\Delta n} = a_0 + a_1\bar{n} + a_2\bar{n}^2$$

Fit \ Parameter	a_0	a_1	a_2	χ^2/dof	comment
1	-0.617×10^{-1}	0.105×10^{-2}	–	5/9	below channel
	$\pm 0.336 \times 10^{-1}$	$\pm 0.22 \times 10^{-3}$			190
2	-0.11	0.14×10^{-2}	–	16/11	all points
	± 0.03	$\pm 0.19 \times 10^{-3}$			
3	0.315	-0.430×10^{-2}	0.187×10^{-4}	7/11	all points
	± 0.149	$\pm 0.195 \times 10^{-2}$	$\pm 0.63 \times 10^{-5}$		

Table 6.4

Results of fits to the data of table (6.4.1) under a variety of conditions

Calibration fit	t_2	$t_2 - t_3$	c	χ^2/dof	Comment
1	0.538 ± 0.168	0.095 ± 0.008	-8.8 ± 12.5	1.58/3	$\bar{n} < 190$
1	0.423 ± 0.025	0.095 ± 0.008	0	2.08/4	$\bar{n} < 190$
1	0.361 ± 0.053	0.092 ± 0.007	5.22 ± 2.93	6.6/7	All points
1	0.447 ± 0.023	0.092 ± 0.007	0	9.7/8	All points
2	0.343 ± 0.049	0.095 ± 0.007	6.9 ± 2.6	4.6/7	All points
2	0.457 ± 0.023	0.095 ± 0.008	0	11.4/8	All points
3	0.285 ± 0.042	0.091 ± 0.007	9.8 ± 2.3	7.1/7	All points
3	0.433 ± 0.023	0.091 ± 0.007	0	24.8/8	All points, one badly fitted
3	$0.308 \pm .045$	$0.092 \pm .007$	7.5 ± 2.76	4.9/6	Badly fitted point excluded
3	$0.413 \pm .023$	$0.093 \pm .007$	0	12.3/7	Badly fitted point excluded

Figure Captions

2.1 A cross section of the core of the apparatus, showing the essential features (a) Si(Li) detector (b) source substrate (c) 2mm thick aluminium detector collimator (d) 1mm thick copper source collimator (e) 0.8mm thick aluminium baffle; a square cut baffle is shown (f) linear motion feed through (g) liquid nitrogen cooled cryopanel (h) teflon centering ring (i) a portion of the vacuum chamber.

2.2 Pileup of the ^{35}S β spectrum on a pulser running well above the end point. The pulser peak occurs at $N = 0$ and reaches 5×10^5 counts/channel. The number of counts/channel is shown for 10 to 169 channels beyond the pulser peak. The solid curve is the form used to represent the toe, added to the low level sum pileup which is visible beyond channel 150. The curve was determined from the data beyond channel 20 and has been extrapolated to channel 1.

2.3 The fraction of low energy pileup as a function of rate. The measurements are consistent with a linear variation, as expected.

3.1 ^{109}Cd calibration spectra for run 12. The upper set of points is the difference between the ^{109}Cd spectrum, which contained both electrons and photons, and a background spectrum from which the electrons had been screened out. The curve shows the fitted electron response function and is a good representation of the data, although the formal quality of fit is appalling, $\chi^2/dof = 13500/723$.

The background is shown as the lower set of points. The prominent feature between $\sim$ 65 keV and 78 keV is identified as due to 88 keV γs Compton scattered into the detector from surrounding material, for the minimum energy of a Compton scattered 88 keV γ is 65 keV (180° scattering) and scattering through 90° yields 75 keV.

3.2 The components of the electron response function are illustrated for an electron energy of 160 keV. The ordinate is the fraction of primary electrons in each 1 keV bin of detected energy. The short range energy loss component (a) is shown for $A_K = 1$ in (3.2.3); 2% of the primary electrons lose more than 5 keV. The long range component (b) is for a slope $S = 0.44$ in (3.3.1); 3% of the primary electrons are found above 100 keV in this component. The flat component (c) is for $F = 4\%$ in (3.4.1) and contains above 100 keV 1.5% of the primary electrons.

4.1 The differences between data and the fitted spectra, in units of the statistical error on each bin, are displayed for all 14 runs. The fits assumed no 17 keV neutrino and the normalisation, end point, energy loss and amount of flat component were varied in the fit. The amount of sum pileup was also a variable.

4.2 The figure shows a ^{109}Cd calibration spectrum for run 9, fitted with inclusion of a peaked baffle scattering term (solid curve). The broken curve is the fit to an equivalent run 12 spectrum (see fig.3.1) and the lower dotted curve shows the fitted component of form (3.6.1). Note the change of scale from logarithmic to linear.

4.3 The summed data from all fourteen runs are shown divided by the best fits achieved with a third order polynomial multiplied by a 17 keV neutrino shape factor. The admixture $\sin^2\theta$ was fixed at zero for (a) and at 0.007 for (b).

5.1 The figure shows numerically calculated residual shape factors
(a) for $\Delta A_K = 0.5$, fitting from 100 keV
(b) for $\Delta A_K = 0.5$, fitting from 120 keV
(c) for $\sin^2\theta = 0.005$, fitting from 100 keV
(d) for $\sin^2\theta = 0.005$, fitting from 120 keV
(e) for $F = 0.05$, fitting from 100 keV
(f) for $F = 0.05$, fitting from 120 keV
The vertical scale shown to the left is to be multiplied by 10 for points beyond 162 keV.

5.2 The figure shows numerically calculated residual shape factors for 5% flat component and 2% of a component peaked at a fractional energy $x = 0.91$,
(a) 2% peaked component, fitting from 100 keV
(b) 2% peaked component, fitting from 120 keV
(c) 5% flat, fitting from 100 keV
(d) 5% flat, fitting from 120 keV
The vertical scale shown to the left is to be multiplied by 10 for points beyond 162 keV.

6.1 The figure shows one example of the shift of the low energy peak in the ^{35}S spectrum as a result of tilting the source. (1) and (3) are one day runs with the normal to the source foil at 40° to the axis of the apparatus. They were separated by a one day run with the source foil perpendicular to the axis (2). Both (1) and (3) peak 25 channels above (2).

6.2 These data calibrate the relation between a peak shift and the change in energy loss responsible. The data points were extracted from the change of the energy loss parameter A_K, determined from ^{109}Cd, from the beginning to the end of a ^{35}S run, and the positions of the low energy β spectrum peak at the beginning and end of a run. Three fits are shown. The solid line is a straight line fit to those points below channel 190. The broken line is a straight line fit to all eleven calibration points. The curve is a parabolic fit to all points.

7.1 (a) Residuals to a straight line fit of the source #2 data over the range shown. The barium K_α signal is prominent in the valley due to the curvature of the β spectrum.

(b) The barium K_α X-ray signal extracted from the summed source #2 data. The data were fitted locally with a second order background and the barium K_α profile; the difference from the smooth background is displayed together with the fitted signal.

Each bin contained approximately 1.1×10^8 counts before subtraction of a smooth background. Typical error bars are shown.

7.2 The figure illustrates our simple model for electrons penetrating a flat plate, in this case from a point on the surface. Half of the electrons, which are emitted isotropically, miss the plate. The others are assumed to pass through a thickness $r = \tau_c / \cos\theta$ for r less than a cutoff r_c. For larger values of θ the thickness of material traversed is $\sim r_c$, independent of θ. The limit r_c would be imposed by the edge of a plate if the plate were small but is more likely determined by multiple scattering.

7.3 The environment of barium L X-rays from a single day of source #1 data taken with high gain. The barium L profile shown contains 2×10^4 counts. The positions of identified or potentially important X-rays are shown. The form of the background under the barium L X-rays is impossible to determine with sufficient accuracy to conclude more than that the number of barium L X-rays probably does not exceed 2×10^4.

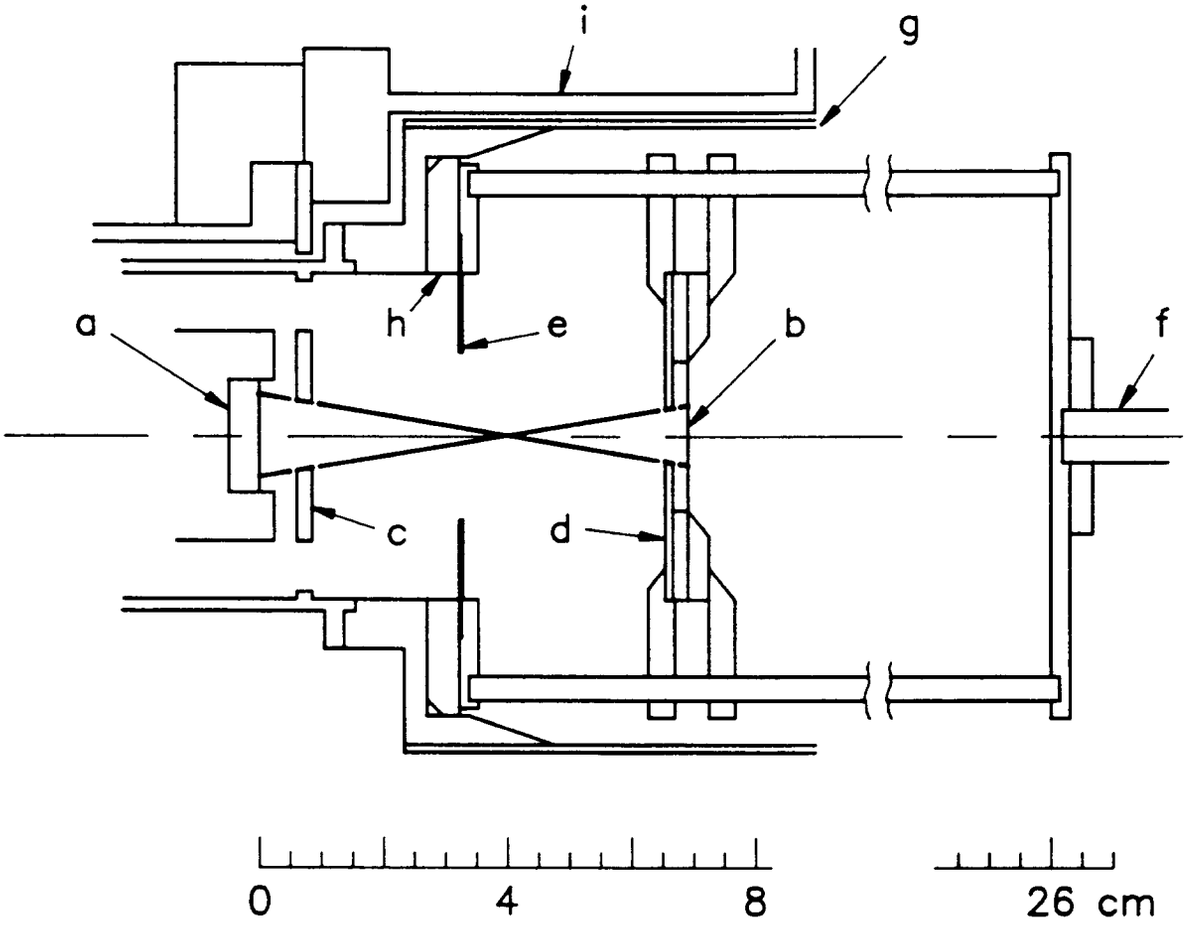

Fig. 2.1

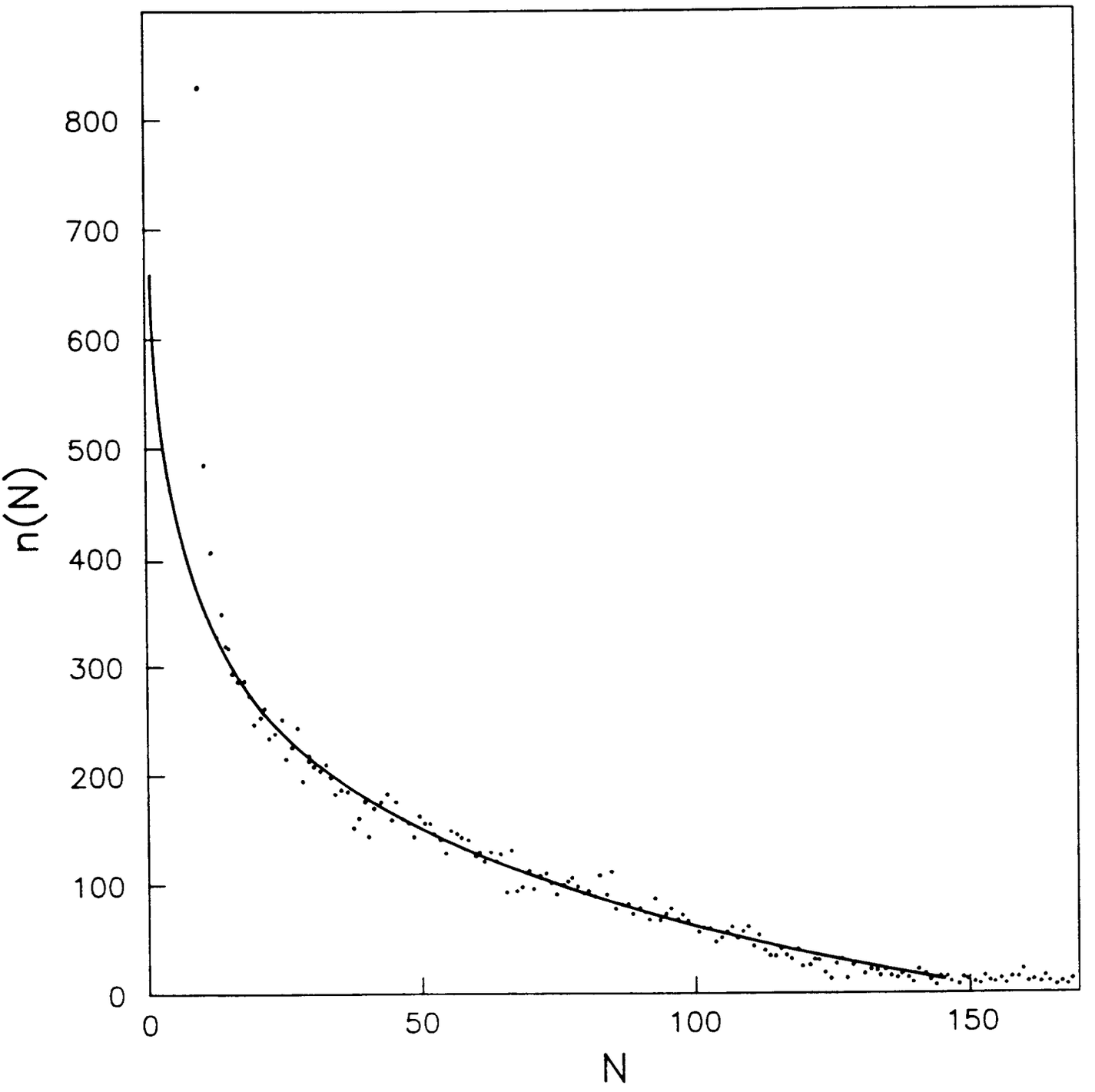

Fig. 2.2

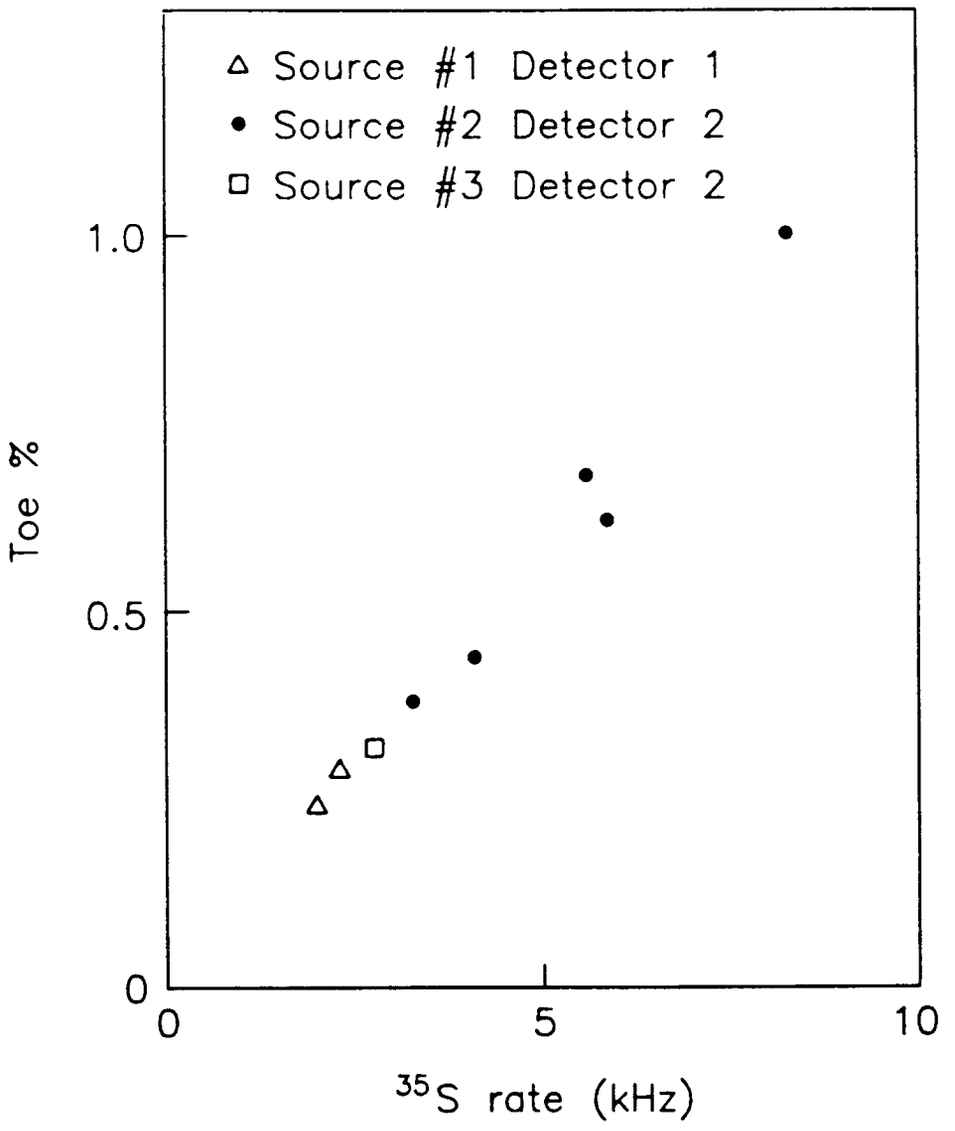
Source #1 Detector 1
Source #2 Detector 2
Source #3 Detector 2
1.0
0.5
0
Toe %
0
5
10
35S rate (kHz)

Fig. 2.3

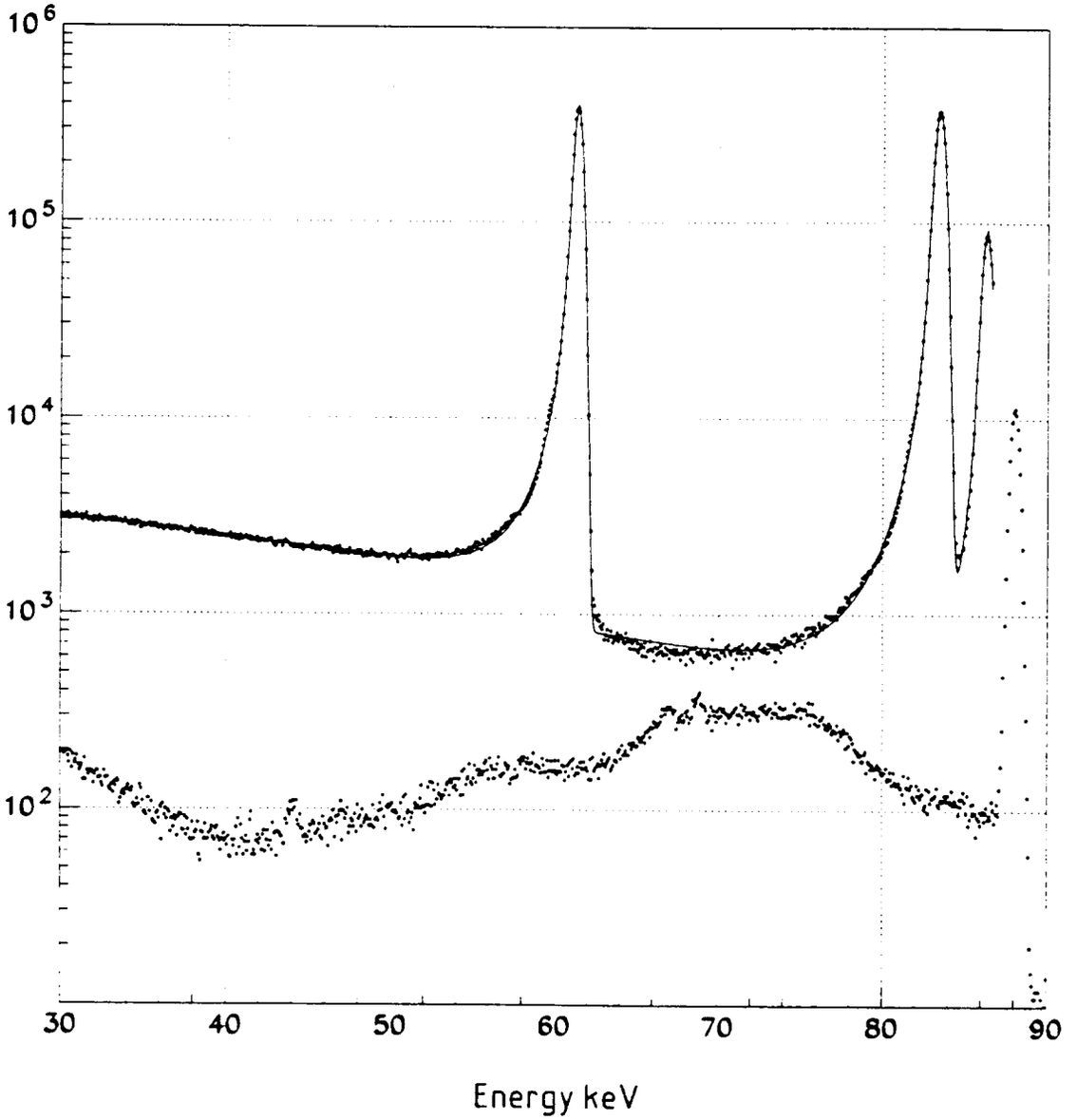

Fig. 3.1

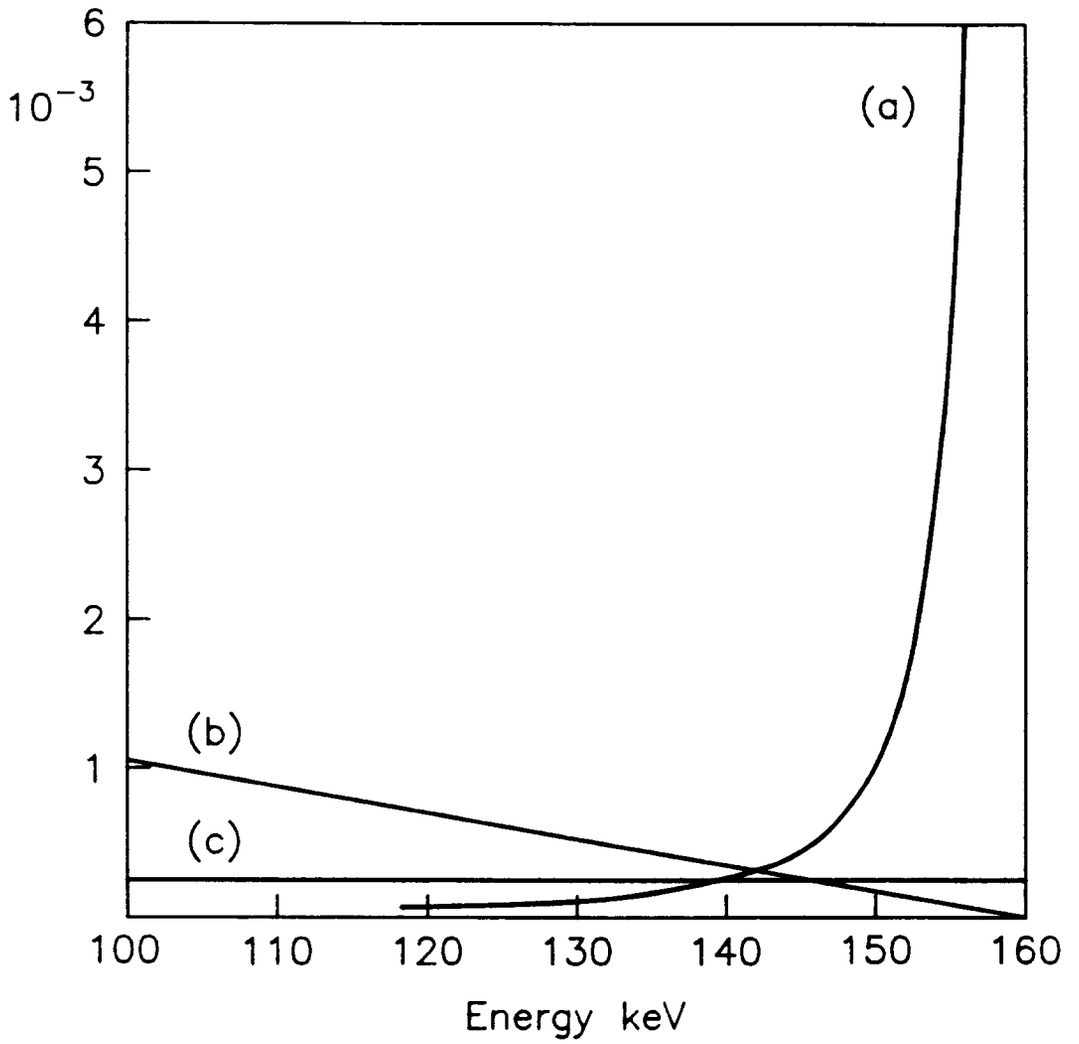

Fig. 3.2

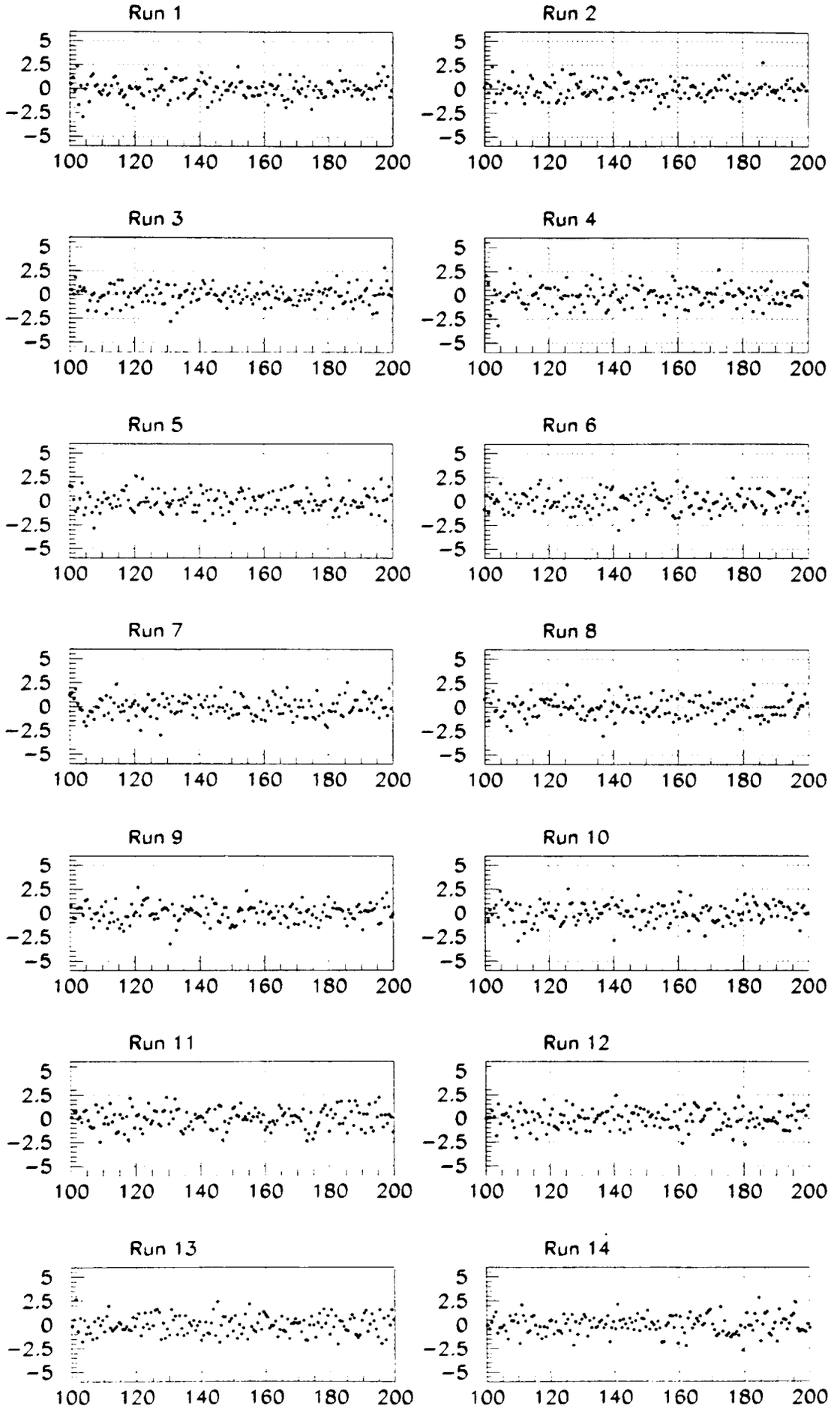
Run 1
Run 2
Run 3
Run 4
Run 5
Run 6
Run 7
Run 8
Run 9
Run 10
Run 11
Run 12
Run 13
Run 14
5
2.5
0
−2.5
−5
100 120 140 160 180 200
Energy keV

Fig. 4.1

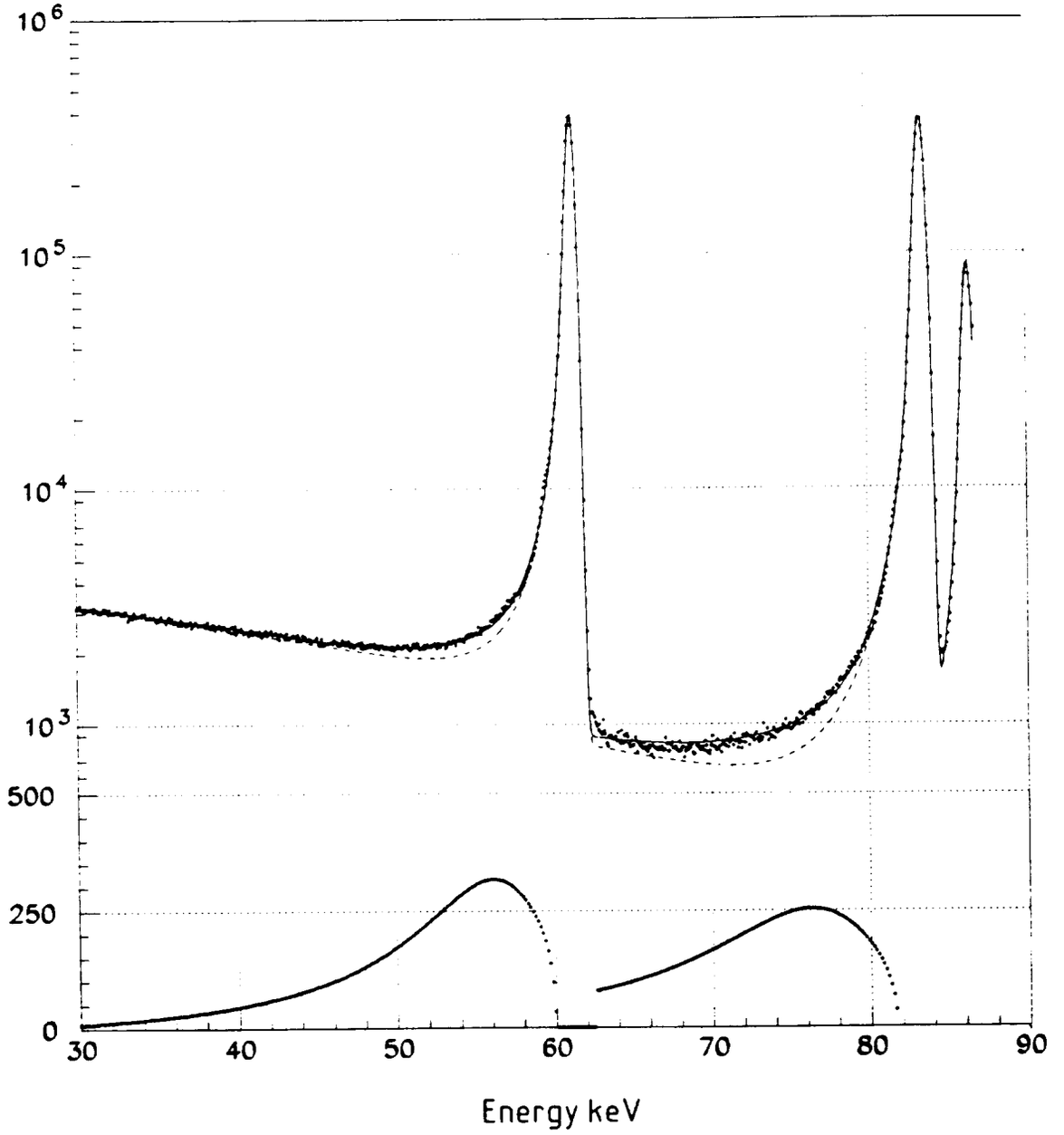

Fig. 4.2

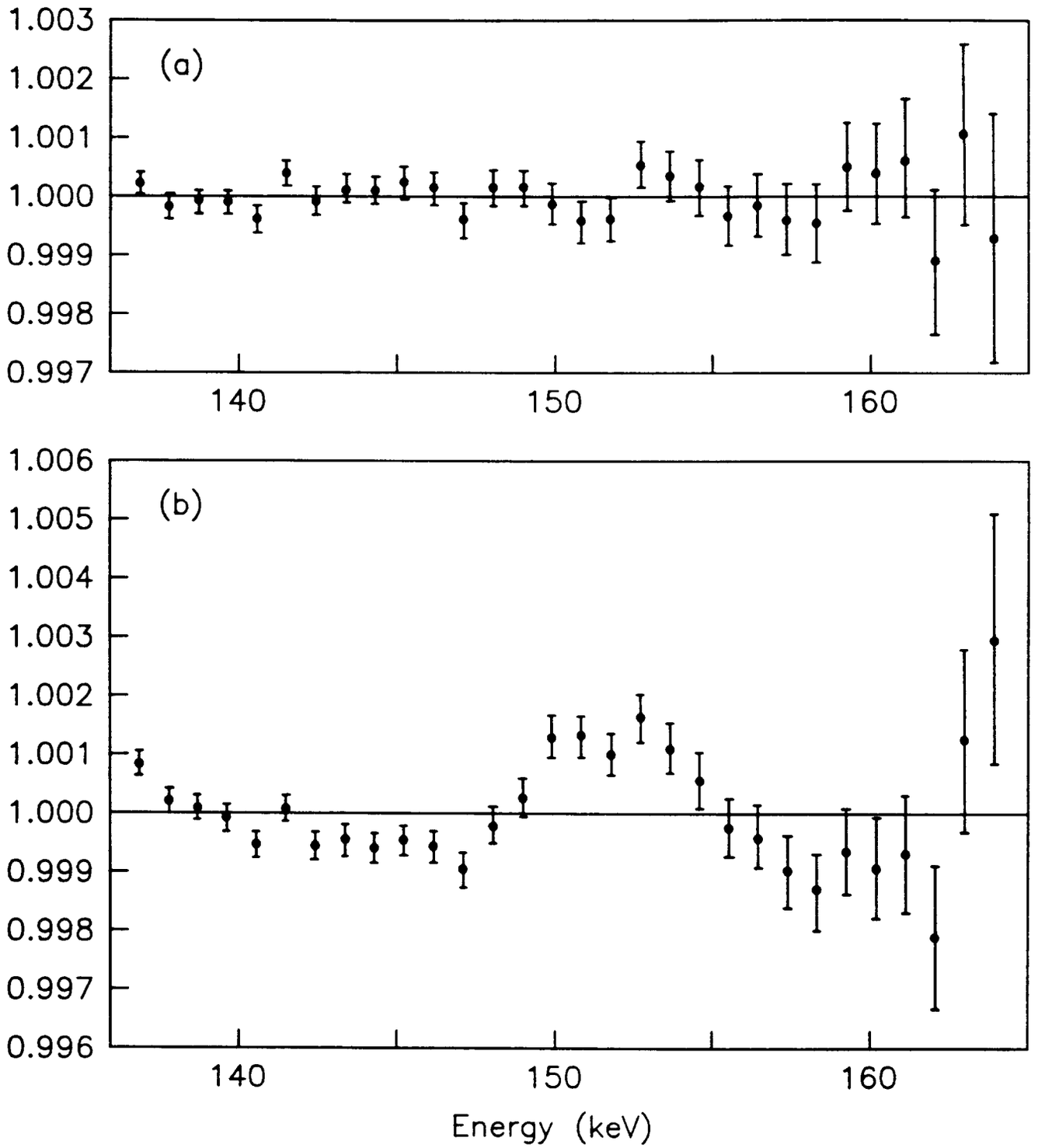
(a)
1.003
1.002
1.001
1.000
0.999
0.998
0.997
140
150
160
(b)
1.006
1.005
1.004
1.003
1.002
1.001
1.000
0.999
0.998
0.997
0.996
140
150
160
Energy (keV)

Fig. 4.3

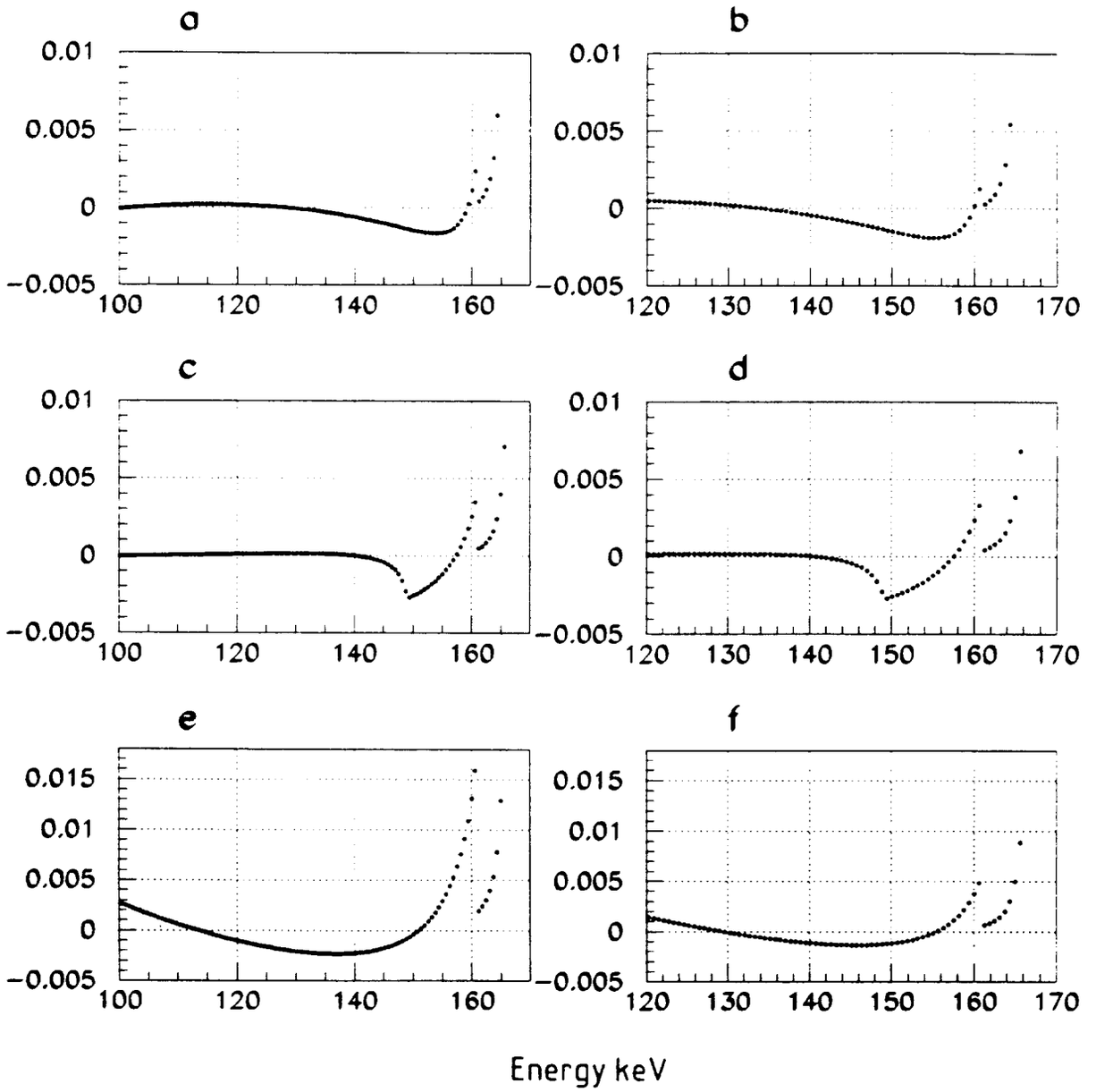
a
b
c
d
e
f
0.01
0.005
0
-0.005
0.015
100
120
130
140
150
160
170
Energy keV

Fig. 5.1

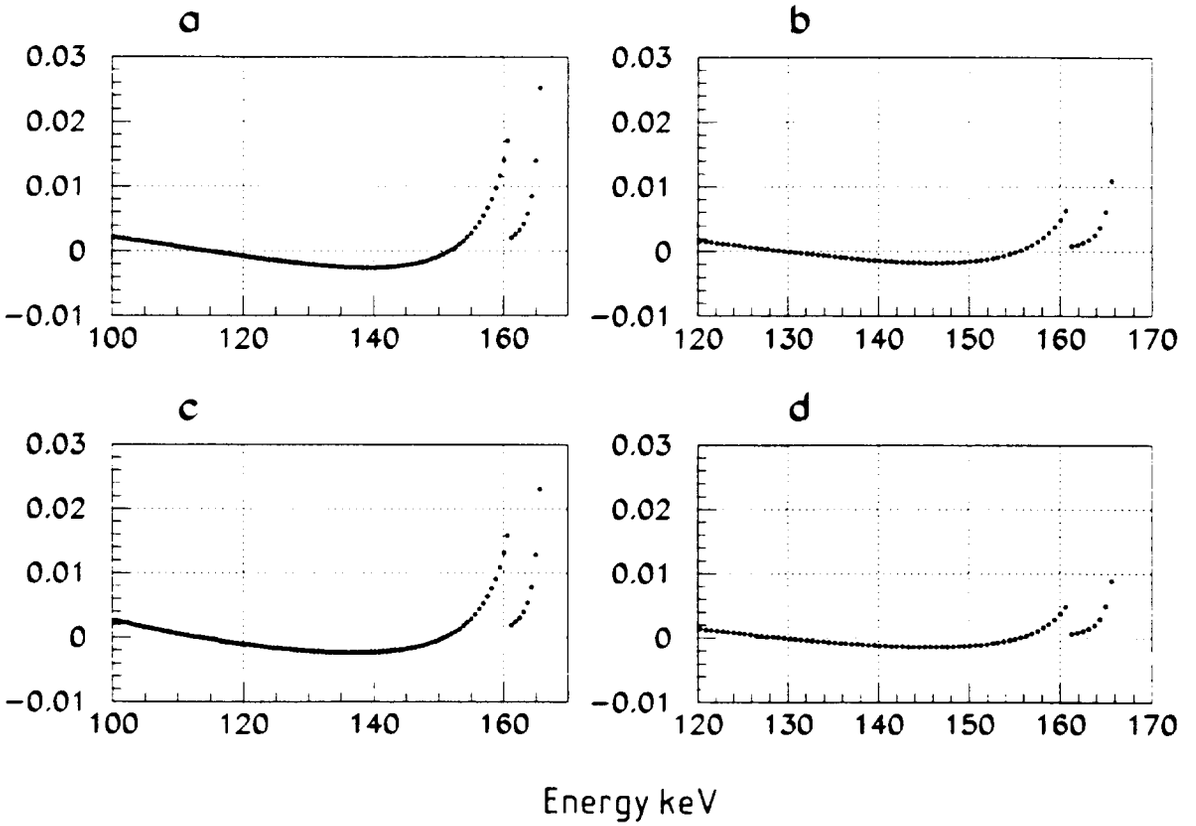
a
b
c
d
0.03
0.02
0.01
0
−0.01
100
120
140
160
120
130
140
150
160
170
Energy keV

Fig. 5.2

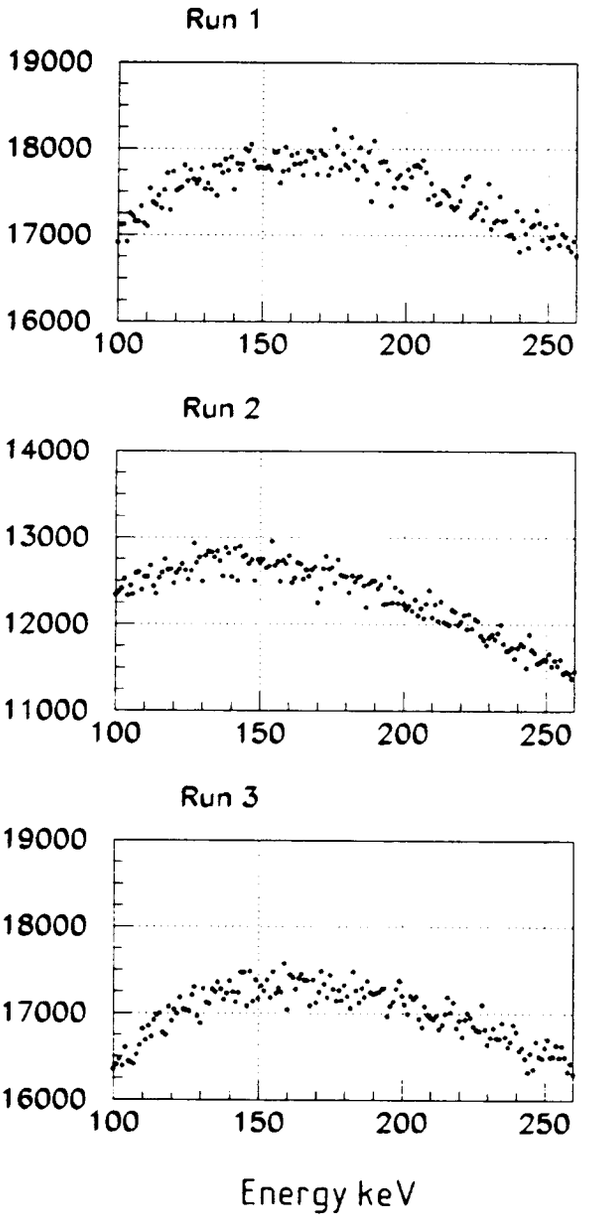
Run 1
19000
18000
17000
16000
100
150
200
250
Run 2
14000
13000
12000
11000
100
150
200
250
Run 3
19000
18000
17000
16000
100
150
200
250
Energy keV

Fig. 6.1

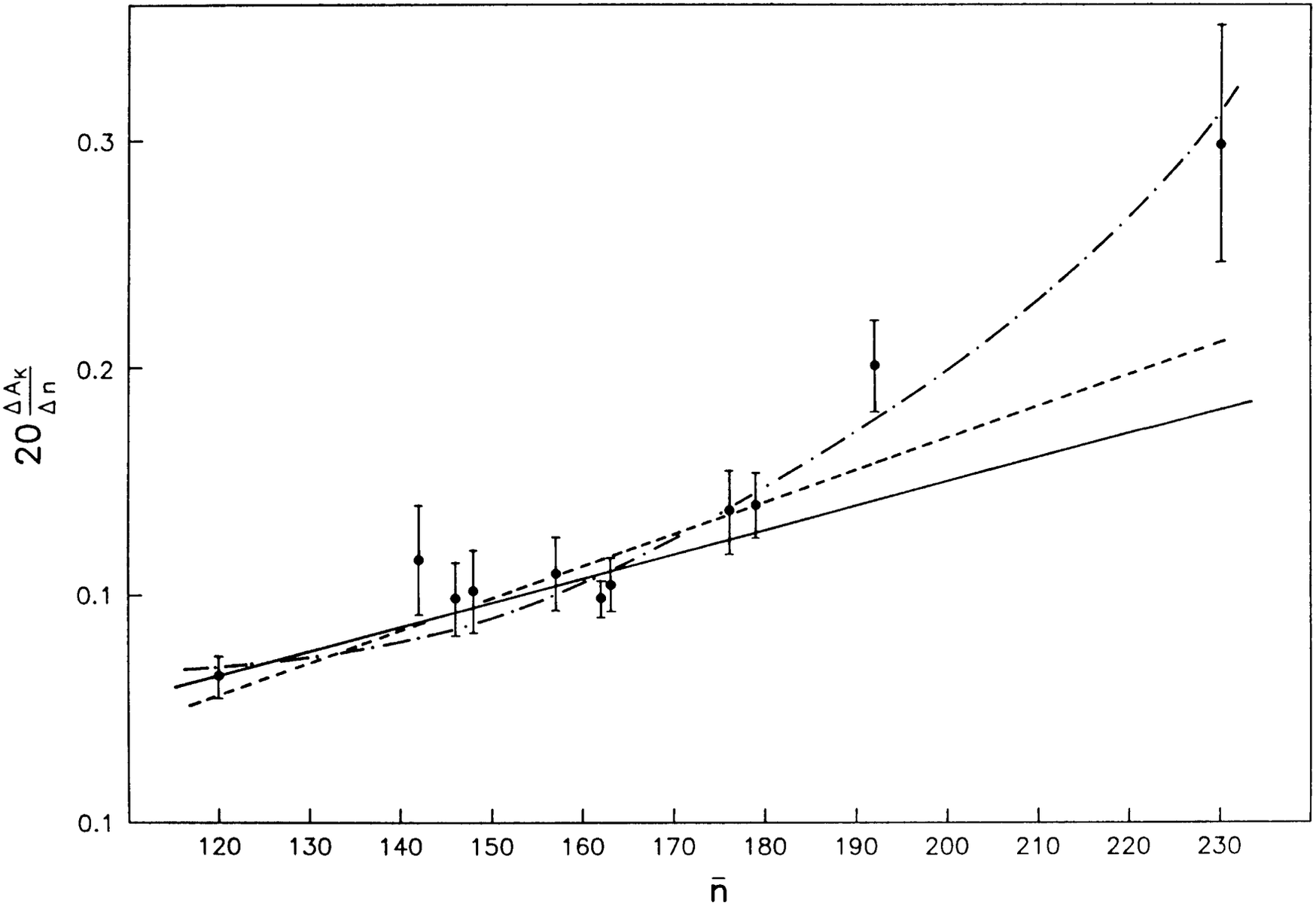
0.3
0.2
0.1
0.1
$20\frac{\Delta A_K}{\Delta n}$
120
130
140
150
160
170
180
190
200
210
220
230
$\bar{n}$

Fig. 6.2

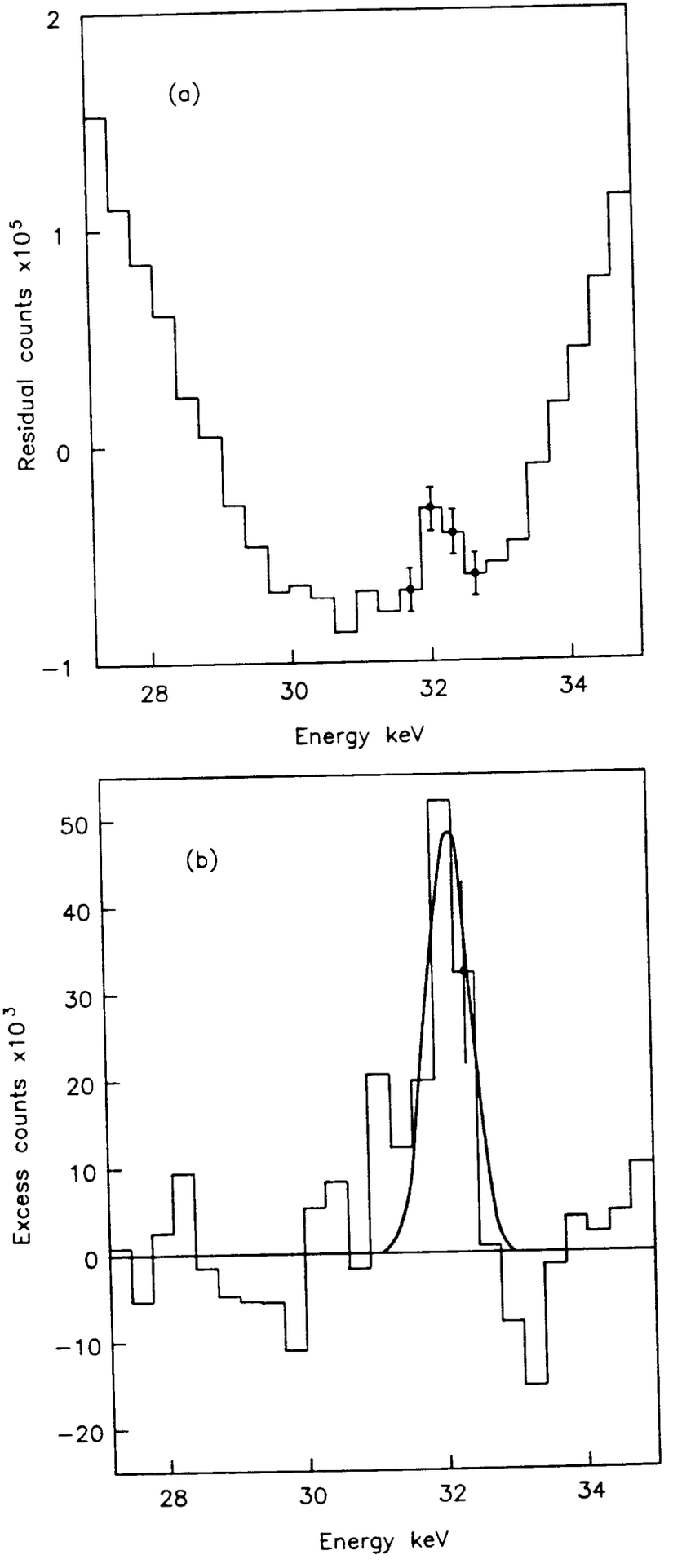
(a)
Residual counts x10^5
2
1
0
−1
28
30
32
34
Energy keV
(b)
Excess counts x10^3
50
40
30
20
10
0
−10
−20
28
30
32
34
Energy keV

Fig. 7.1

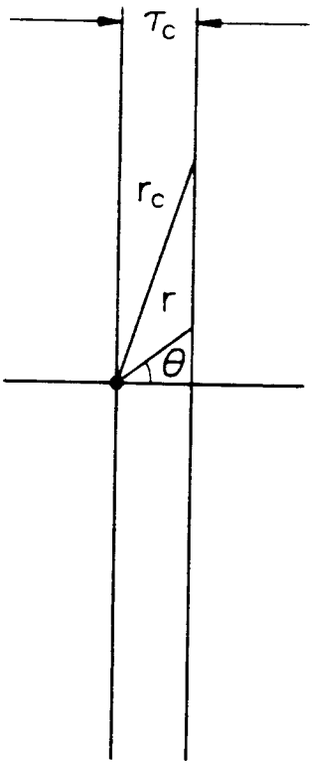

Fig. 7.2

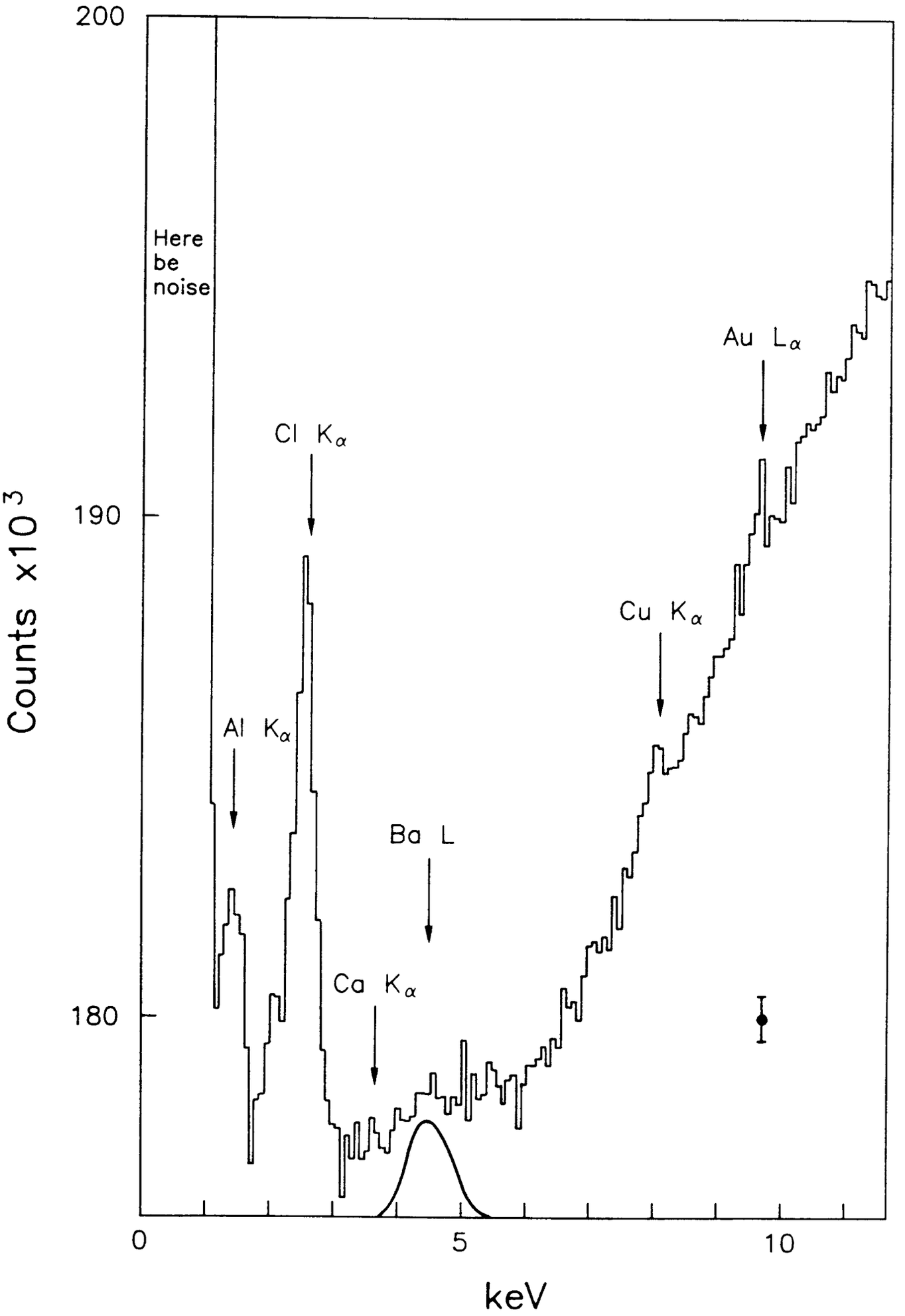
200
190
180
Counts x10^3
Here be noise
Cl K_α
Au L_α
Cu K_α
Al K_α
Ba L
Ca K_α
0
5
10
keV

Fig. 7.3